UCRL-9944
UC-4 Chemistry
TID-4500 (16th Ed.)

UNIVERSITY OF CALIFORNIA

Lawrence Radiation Laboratory
Berkeley, California

Contract No. W-7405-eng-48

MAGNETIC RESONANCE OF METALS AND PARAMAGNETIC IONS IN SOLUTION

Judith Brown

(Thesis)

December 13, 1961

Printed in USA. Price $1.50. Available from the
Office of Technical Services
U. S. Department of Commerce
Washington 25, D.C.

DISCLAIMER

MAGNETIC RESONANCE OF METALS AND PARAMAGNETIC IONS IN SOLUTION

Contents

MAGNETIC RESONANCE OF METALS AND PARAMAGNETIC IONS IN SOLUTION

Judith Brown

Lawrence Radiation Laboratory
University of California
Berkeley, California

December 13, 1961

ABSTRACT

Several methods of conducting electron spin resonance experiments at temperatures up to 600°C are described. The system lithium in lithium iodide was studied in an attempt to observe the resonance of lithium metal dissolved in molten lithium iodide. No resonance was observed, from which it is deduced that $T_2 < 2 \cdot 10^{-10}$ sec. The relaxation times and g values of lithium metal in lithium iodide were measured at temperatures below the lithium iodide melting point. There was no variation of g value, but the relaxation time at 425°C is greater than its room-temperature value by approximately 20%. The line shape was found to vary with temperature and to depend upon sample treatment prior to measurement.

Electron spin resonance measurements of the line width of ultraviolet-irradiated lithium hydride at temperatures greater than 25°C were made in order to test the hypothesis that the line arises from colloidal lithium metal. The intensity of the line was drastically reduced at 95°C, and the line had disappeared completely at 170°C.

Electron spin resonance studies were conducted from 25°C to 500°C on the systems $MnCl_2$, $MnCl_2 \cdot 4H_2O$, $MnCl_2$ in $ZnCl_2$, $MnCl_2$ in LiCl-KCl, $CrCl_3$, $CrCl_3$ in $ZnCl_2$, $CrCl_3$ in LiCl-KCl, $NiCl_2$ in LiCl-KCl, $FeCl_3$, $FeCl_3$ in LiCl-KCl, and $VOCl_2$ in LiCl-KCl. In the solutions resonances were observed only in Mn(II) and Cr(III). For Mn(II) solutions the line width decreases with increasing temperature and increasing concentration. The concentration effect is due to exchange narrowing, and it is shown that the exchange phenomenon is still significant at a concentration of 0.3 M. Our results in Mn(II) solutions are compared with several theories of relaxation in liquids, with poor agreement. No variation of line width with temperature was observed in solutions of Cr(III). In addition, the line width was found to be the same for the Cr(III) solutions as for the mixed powders of the same concentration. Some interesting temperature effects encountered in the solids are reported.

Although the problem is chemically appealing, a more careful consideration of the resonance properties to be expected from such a system indicates quite a number of unfavorable conditions. For the most part these ions would not be in S states, which implies a line broadening due to both the dipole-dipole interaction and the spin-orbit interaction, which would shorten the spin-lattice relaxation time. This, of course, assumes that the orbital angular momentum would not be "quenched." Probably the orbital contribution would be small, but even so it could provide an effective relaxation mechanism. The viscosity of most molten salts is slightly greater than that of water. This means that the correlation time[3] would be increased, also leading to a broader line. There is in addition the problem of the rapidly fluctuating electric (and, therefore, magnetic) fields seen by an ion because of its ionic environment. These would almost certainly have Fourier components at the proper frequency to cause spin flips and again decrease the spin-lattice relaxation time.

However, even in view of the above observations, the most convincing argument against success with this type of system lies in the fact that the susceptibilities have been measured by the Guoy method and found to be diamagnetic for all cases of sufficient solubility for measurement. This would imply a small amount of paramagnetism, if any. The lead system given as an example above is predicted, on the basis of an early EMF measurement,[4] to be paramagnetic, but here the solubility (only 0.024 mole % at 438°C) would be insufficient for detection except in the case of an extremely sharp resonance line.

In view of these difficulties, it was decided that solutions of alkali metals in their metal halides offered greater possibilities for successful resonance experiments. Although much more difficult from the point of view of sample preparation and temperature required, these solutions would contain s electrons and would almost certainly be paramagnetic. One might even predict the type of results to be obtained from the different species speculated.

Consider, for example, the system Li in LiI. This was chosen for experiments because of the relatively low LiI melting point. For isolated lithium atoms with a localized electron on each atom, one would expect to see four lines arising from the hyperfine interaction with the Li nuclear spin I = 3/2.* (This isotope is 93% abundant.) The subhalide species would here involve Li_2^+, and one should find seven lines arising from the interaction with the two nuclei. The species Li_2 would be diamagnetic. Finally, electrons in a conduction band would give rise to a single line, as would a chemical exchange of

$$Li + Li^+ = Li^+ + Li$$

were it more rapid than the hyperfine-interaction frequency ($2.5 \cdot 10^9$ $\overline{\text{sec}}$).

*The coupling constant is predicted to be 145 gauss from atomic beam measurements. See W. D. Knight, Solid State Physics 2, 93 (1956).

Previous work on alkali metal-alkali halide systems has consisted chiefly of phase diagrams and has been carried out by Bredig and co-workers at Oak Ridge.[5] A typical phase diagram, this for the system K-KCl, may be found in Fig. 1.

In our opinion the most interesting papers have been those on the electrical conductivity of potassium and sodium metal in their metal halides[6] and of the metal-rich KI-in-K system.[7] The results of the former (see Fig. 1) were discussed in terms of the equivalent conductance of the metal in solution; $\Lambda \equiv \kappa\, Ve$, where Λ is the equivalent conductance, κ the specific conductivity, and Ve the volume in milliliters containing 1 equivalent of solute.

To calculate the equivalent conductivity, additivity of volumes and additivity of equivalent conductances were assumed. The latter has not been observed in mixtures of molten salts reported in the literature and is therefore a poor approximation; however, it does give an indication of the effect of the addition of the metal and is a useful concept in this sense.

It was felt that the variation of conductivity with temperature would offer a greater insight into the nature of the solutions. Therefore, we have made a very rough estimate of the temperature coefficient of conductivity,

$$\frac{\Delta\kappa}{\kappa} \quad \frac{1}{\Delta T} \quad 100,$$

from Bredig's data at 760°C and 870°C for the system K-KBr. This we plotted against the reciprocal concentration, assuming a linear variation of conductivity with temperature over this range. This is a fairly good approximation for ionic conductivity, although an examination of Bredig's curves indicates that it is by no means exact. The results are compared with those for K in liquid NH_3,[8] where the rapid decrease of the temperature coefficient of conductivity at a concentration of approximately 1.5 M corresponds to the establishment of a metallic conduction band. (See Fig. 2.) The obvious conclusion is that even with a concentration of 20 mole % K in KBr we are not yet in the region of metallic conduction. In fact, an examination of Fig. 1 of Ref. 7 indicates that the establishment of metallic conduction is very gradual, beginning at a concentration of approximately 65 mole % K for the K-KI system and not becoming truly predominant until approximately 95% K.

For completeness and to give an idea of the orders of magnitude involved we include Table I.

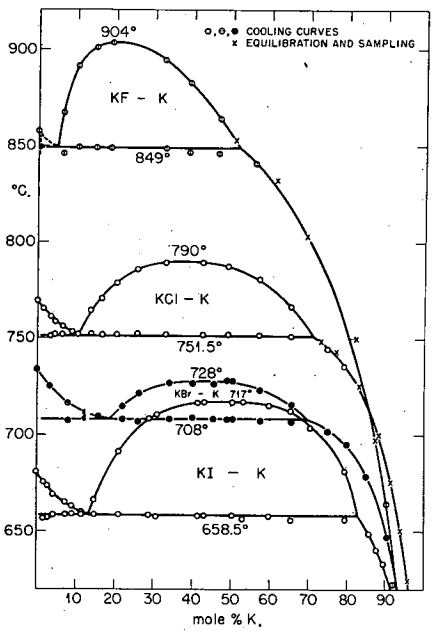

—Temperature–composition phase diagrams of the KX–K systems.

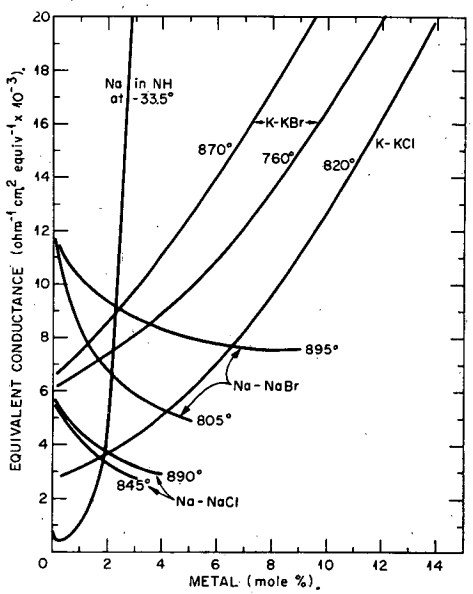

—Equivalent conductance of sodium and potassium metals in their molten chloride and bromide solutions.

MU-25112

Fig. 1. (left) Reproduced from J. W. Johnson and M. A. Bredig, J. Am. Chem. Soc. 62, 604 (1958) by permission of The American Chemical Society. (right) Reproduced from Ref. 6 by permission of The American Chemical Society.

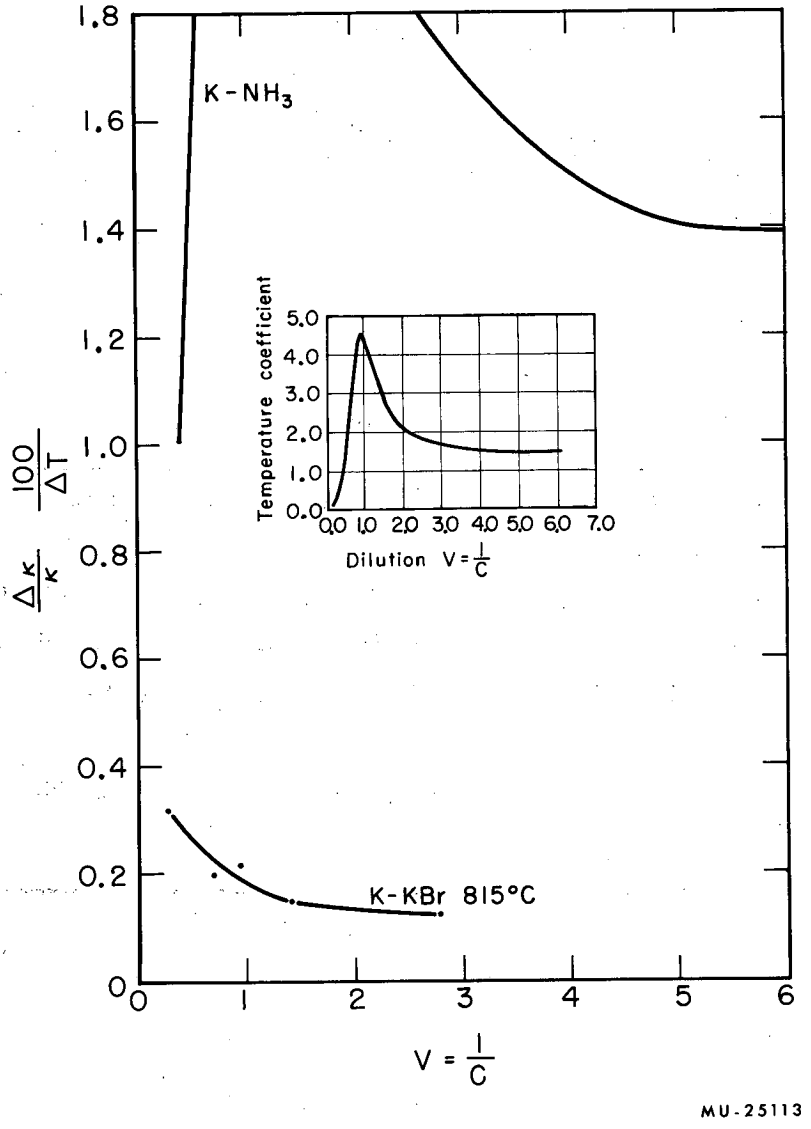

Fig. 2. Temperature coefficient of conductivity for K-KBr and K-NH_3. Inset reproduced from C. A. Kraus and W. W. Lucasse, J. Am. Chem. Soc. 45, 2551 (1923) by permission of The American Chemical Society.

Table I. Conductivities and equivalent conductances.

	Temperature (°C)	κ (mho cm^{-1})	Λ (mho cm^2)
NaCl	800	3.55[a]	133.2[a]
Na	300	$5.78 \cdot 10^4$ [b]	$1.02 \cdot 10^6$ [d]
	800	$3.08 \cdot 10^4$ [b]	$1.91 \cdot 10^6$ [d]
8% K-KBr	800	22 [c]	14900 (Λ of metal)
K	300	$3.54 \cdot 10^4$ [b]	$2.12 \cdot 10^6$ [d]
	800	$1.86 \cdot 10^4$ [b]	$1.12 \cdot 10^6$ [d]
KBr	800	1.74 [a]	100.5 [a]
LiF	850	14.8[a]	
	950	24.8[a]	

a. B. E. Conway, Electrochemical Data (Elsevier Publishing Company, Amsterdam, 1952).

b. N. Cusack and J. E. Enderby, Proc. Phys. Soc. 75, 395 (1960). The values at 800°C represent an estimate which was made from equations in this reference outside the range of validity quoted.

c. Estimated from Ref. 6.

d. Calculated from data in (b) by using molar volumes of Na and K equal to 33 ml and 60 ml respectively.

B. Experimental Method

The most obvious requirement for execution of this problem was a means of conducting electron spin resonance measurements at temperatures of at least 450°C, with still higher temperatures of great advantage. Several methods were worked out; these are discussed in order of application.

1. TE_{102} cavity

Initially a simple full-wave rectangular stainless steel cavity was constructed of Type 304 stainless steel wave guide obtained from Pacific Tube Company. The heater[9] was a quartz tube wrapped noninductively with 10-mil-diameter platinum–10% rhodium wire. The wires were held in place by a cement of ZnO and water glass. In designing this cavity it was discovered that several well-known high-temperature cements are paramagnetic. This cavity had a Q of only 2000, but the principal difficulty lay in a broad false signal centered at g = 2. This is now believed to have arisen from iron in the stainless steel wave guide and an imperfect plating job, which was only slightly improved after several plating attempts.

2. TE_{011} cavity

The TE_{011} cylindrical cavity was constructed in an attempt to attain greater sensitivity; in general, cylindrical cavities have a higher Q, as the ratio of volume to surface upon which Q depends is greater. Also, some other minor problems encountered with the earlier apparatus were corrected.

This cavity (see Figs. 3 and 4) consisted of a quartz cylinder silvered with Du Pont de Nemours Product No. 4545, with the top and bottom of conventionally silver-plated brass plates held together by 4/40 screws. An adaptor, which could be used to hold coupling windows in place, fitted into the upper plate. This was pressed down firmly by a piece of wave guide, and these parts were screwed into tapped holes in the upper plate. The choice of quartz for the cavity was due to its low coefficient of thermal expansion. A slight inconvenience had arisen in the rectangular cavity from the change of dimensions with temperature, causing a drift off the resonance frequency. There was the additional advantage that this system could be used with high-frequency modulation where skin depth considerations prohibit the use of a metal cavity. However, this technique was not employed here.

The relationship between the resonant frequency and cavity dimensions for a $TE_{\ell mn}$ cylindrical cavity is[10]

$$(fD)^2 = \left(\frac{cx_{\ell m}}{\pi}\right)^2 + \left(\frac{cn}{2}\right)^2 \left(\frac{D}{L}\right)^2 ,$$

where L is the length of the cylinder, D the diameter and ℓ, m, and n are defined as follows:

ℓ = number of full-period variations of E_r with respect to θ,
m = number of half-period variations of E_θ with respect to r,
n = number of half-period variations of E_r with respect to z.

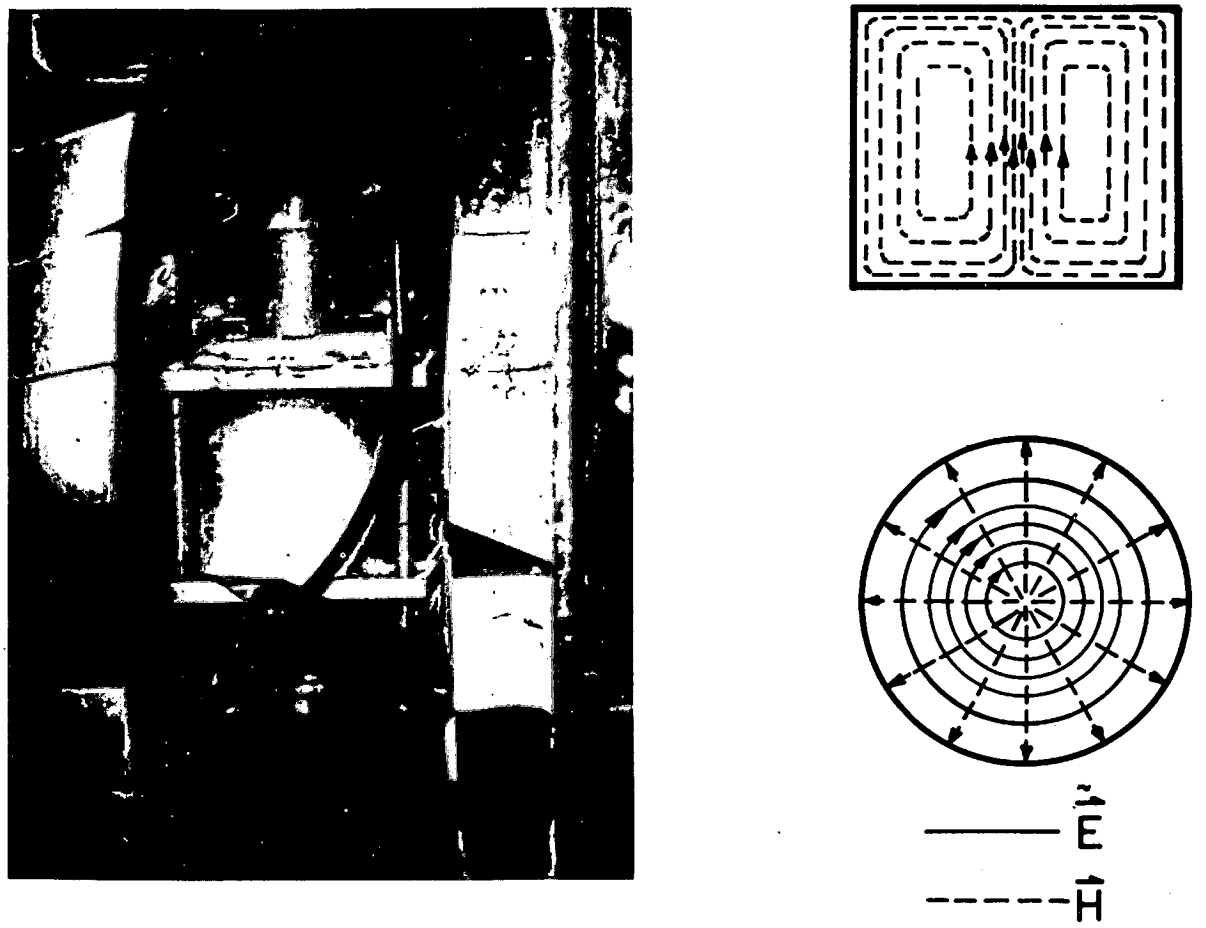

Fig. 3. TE_{011} cylindrical cavity and cross section showing TE_{011} mode.

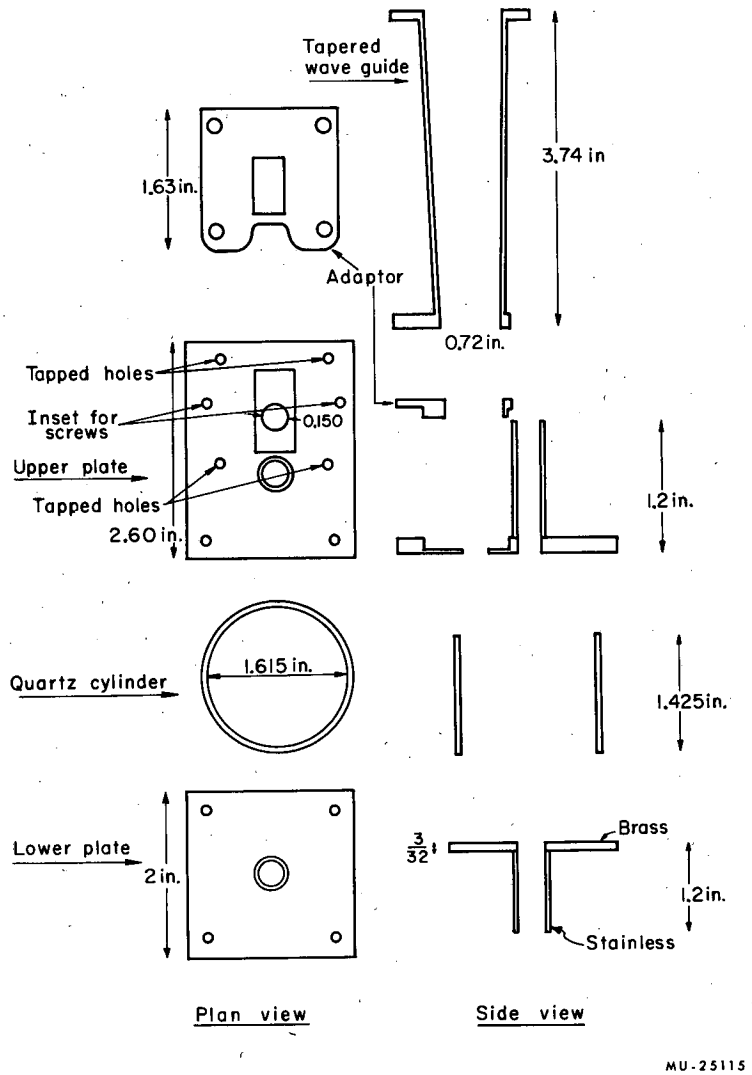

Fig. 4. TE_{011} cavity parts.

Further, $X_{\ell m}$ is the mth root of $J'_\ell(X) = 0$ with values tabulated in Montgomery. This is simply an equation for the position of the nodes in the z direction in a piece of cylindrical tubing, and can be derived by solving the wave equation obtained from Maxwell's equations and the relationships, $\vec{B} = \mu\vec{H}$, etc., imposing metallic boundary conditions. See Townes and Shawlow for a clear discussion.[11]

The heater consisted of a quartz tube platinized in two strips with Hanovia Chemical Company's Liquid Bright Platinum No. 5; this was similar to an arrangement described recently by Singer.[12] A current of 5 amp from a regulated dc power supply gave a temperature of approximately 500°C. This heating method was advantageous in that microphonic noise due to vibration of the wires in the previous apparatus was eliminated. Temperatures were measured by a platinum–platinum-10% rhodium thermocouple inserted into the sample-containing quartz tube just outside the cavity. A calibration of sample temperature vs temperature measured was made by using two thermocouples, one in a glass capillary at the normal sample position.

The only real problem encountered with this apparatus was in coupling microwave power into the cavity. In general with a cylindrical cavity of this type one couples from the center of the wave guide where the power is a maximum into the side of the cylinder. However, the use of quartz necessitated coupling into the top; and the position of the side arm which held the heater and the side of the cylinder determined the position of the coupling hole, which was off center for the wave guide. It was found that when the heater, the inner quartz tube to hold the sample, and the sample itself were in place, an insufficient amount of power was coupled into the cavity. This difficulty was solved by use of a piece of wave guide tapered to 0.72 in. (see Fig. 5), which is just over the cutoff wave length at 8300 Mc, placing the coupling hole more nearly in the center.

The unloaded Q of this cavity was too high to measure accurately with a wave meter,* but is estimated at 10,000 at a resonant frequency of 9512 Mc. With the heater in place this decreases to $\nu_0 = 9380$ Mc and $Q \geq 6000$.

3. Terminated Wave Guide

It was discovered that a cavity system is not well suited to the study of very lossy samples such as molten salt solutions. In such a case of large energy dissipation the cavity Q, which is defined as (2π Energy stored/Energy dissipated per cycle), and therefore the resulting sensitivity are drastically reduced.

---

*The quantity measured is $\nu_0/\Delta\nu$, where ν_0 is the resonant frequency and $\Delta\nu$ is the width in frequency between the points at which the power absorbed is 0.707 of its value at resonance.

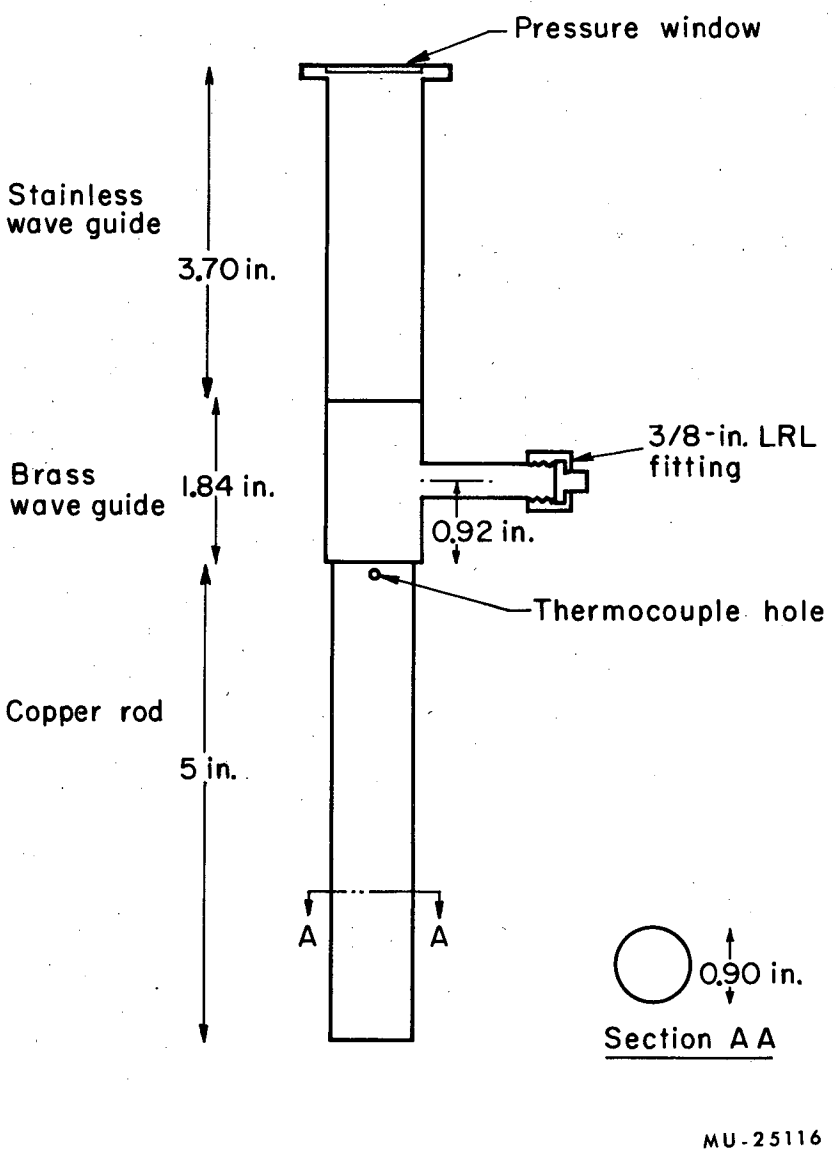

Fig. 5. Terminated wave guide.

Accordingly, a much simpler system* consisting of a section of wave guide terminated by a copper block was constructed. This copper block could be heated by a circular ceramic furnace outside the magnet gap. See Fig. 5. The lower portion of the wave guide, containing the sample at the bottom, was of brass, as stainless steel was found to give rise to a broad false signal. The upper portion, however, was of stainless steel wave guide because of its lower coefficient of thermal conductivity. Owing to the extreme reactivity of the sample, it was necessary for the system to be air-tight; this was accomplished by means of a pressure window (Microwave Associates Inc.) soldered into the upper flange.. The sample could be introduced by means of the side arm positioned one-half wave length above the termination. The inside of the apparatus was silver-plated a thickness of approximately 5 mils to prevent reaction with the extremely corrosive samples.

Temperatures were measured by means of a platinum–platinum-10% rhodium thermocouple inserted into a small hole in the copper block just below the sample. The temperature measured was found to be approximately equal to the sample temperature. The error is estimated as ± 5°C as an upper limit, and is probably less.

Almost all the experiments with this apparatus were conducted at a frequency of 9400 Mc and at maximum klystron power estimated as 200 to 250 milliwatts.

4. Electron Spin Resonance Spectrometer

A conventional X-band spectrometer with the usual balanced bridge arrangement was used for these measurements. A block diagram of the apparatus, which is largely self-explanatory, can be found in Fig. 6. The microwave source was a Varian V 58 klystron stabilized by a Laboratory for Electronics unit. The magnetic field was provided by a Varian 6-inch magnet and associated stabilized power supply.

Line widths and g values were measured with a proton resonance probe and marginal oscillator-detector. The output of the oscillator was fed into a Hewlett-Packard frequency counter and an oscilloscope on which the proton resonance was observed. By varying the oscillator frequency it was possible to mark the proton resonance frequency at regular intervals while varying the dc field, yielding an absolute field measurement. A correction for the difference in probe position and sample position was made by comparison to the resonance frequency of DPPH, taking $G_{DPPH} = 2.0036$.

5. Sample Preparation

Preparing samples for the measurements with the TE_{011} cavity was in itself quite a formidable task. Ordinarily electron spin resonance measurements are made upon samples contained in glass capillaries. However,

*We should like to thank Professor Rollie J. Myers for this suggestion.

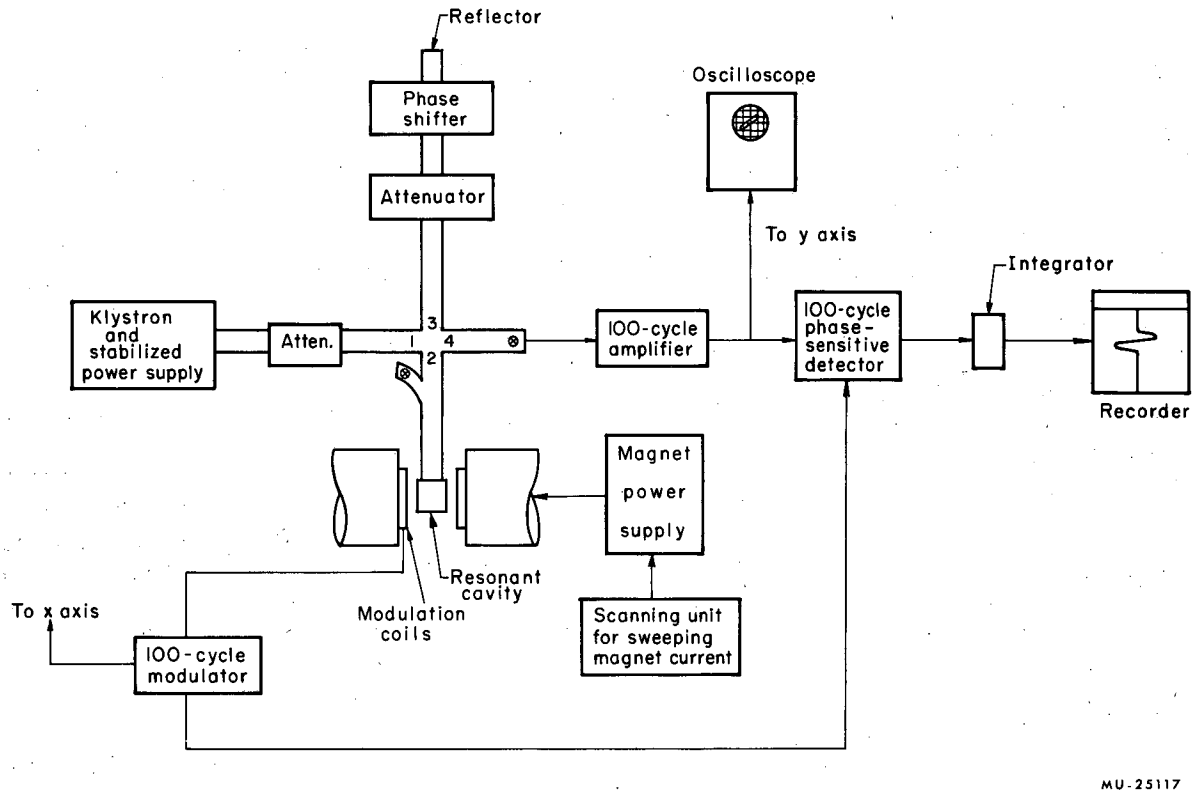

Fig. 6. Block diagram of electron spin resonance spectrometer.

the alkali metals attack glass, bycor, and quartz. Lithium metal is particularly difficult to work with, as it also attacks BeO_2 and Al_2O_3 or sapphire. In addition, all work must be done in an inert atmosphere or vacuum.

Initially, an attempt was made to distill the metal into a thick-walled capillary, add the salt, and conduct measurements before the metal had eaten through the wall. As might be expected, this method proved unsuccessful. However, it was found possible to distill lithium metal from a tantalum crucible contained in a glass tube; and this preparation actually gave the sharpest resonance line, indicating the highest degree of purity encountered in this work.

A more successful procedure involved loading the Li and LiI onto a silver foil boat, which was then sealed in a quartz tube. This procedure was carried out in a dry box under a nitrogen atmosphere and worked adequately.

The sample preparation for the terminated wave guide apparatus involved more difficulties in terms of seemingly ubiquitous water vapor. This was easily detected during the course of an experiment, as the balanced bridge became rapidly unphased on passing through the boiling point of water. Eventually, an evacuatable argon box was employed; this system was pumped down to approximately 60 μ Hg with all necessary equipment inside. Argon (Linde Company) was passed in and the actual loading of the sample accomplished.

Lithium metal obtained from the Lithium Corporation of America and purified anhydrous LiI obtained from City Chemical Corporation were used in these experiments. The LiI was, in addition, dried in vacuum at 400°C until a pressure of less than 10^{-4} mm of mercury was reached. The lithium metal was stored under an organic solvent and then evacuated before being placed in the dry box for preparation of the samples.

C. Experimental Results and Discussion

1. TE_{011} Cavity

Experiments conducted upon Li in LiI before formation of the metal–metal halide solution yielded line shapes characteristic of particles greater than the skin depth.* The relaxation time T_2 was estimated as $7(\pm 2) \cdot 10^{-9}$ sec. Feher and Kip reported relaxation times ranging from $3 \cdot 10^{-9}$ to $2.5 \cdot 10^{-8}$ sec, depending upon the purity of the sample.[13] This indicates that our metal was of less than the attainable purity, but this was not considered of drastic importance for the purposes of this experiment.

*See Appendix for a discussion of the line shape in conducting media.

After formation of solution (i.e. heating to 500°C) and subsequent cooling to room temperature, the line shapes had the symmetric Lorentz form usually encountered in ESR experiments (see Fig. 7). This is interesting in that it implies solution formation followed by a precipitation of colloidal metal particles of dimensions less than the skin depth ($1.6 \cdot 10^{-4}$ cm) upon cooling. To our knowledge there has been no study of this phenomenon for alkali metal–metal halide solutions, although it is known to occur for the nonalkali metal systems.[2]

The lithium metal resonance, easily observable at room temperature, could be followed (with greater difficulty at higher temperature) to the melting point of the lithium iodide (438°C). Here, unfortunately, a very lossy solution was formed with a resulting loss of sensitivity, as mentioned earlier. And, as the salt-rich metal–metal halide solutions were of primary interest in this work, a novel approach was necessitated.

2. Terminated Wave Guide

The experiments and results described herein are essentially the same as those above. However, the experiments were more carefully executed, and these latter results are believed due to the inherent properties of the system under study rather than a lack in sensitivity of the apparatus.

Examples of the line shape as a function of temperature are found in Fig. 8. It is evident that the asymmetry parameter A/B (defined in Fig. 33) decreases with increasing sample temperature. At 266°C the value 2.3, expected in the limit of slowly diffusing dipoles, is found; whereas at 390°C the line shape is actually symmetric, implying that the sample dimensions are less than the skin depth.

This reduction in T_D could be explained in two ways. Either the conductivity is drastically reduced owing to the dissolution of LiI in the Li metal, or the lithium metal diffuses into the salt to yield particles of dimensions less than the skin depth. If we make an analogy with the NaI-Na system, the solubility of LiI in Li would be less than 1 mole % at the highest temperatures studied. However, even a small amount of LiI might be very effective in reducing the conductivity of the lithium metal. We shall await further data from Bredig and co-workers to elucidate this point.

Our data on T_D as a function of temperature could be utilized more completely if the phase diagram of the system and conductivity as a function of temperature and concentration were known. Dyson's theory (see Appendix) predicts

$$T_D \propto \frac{1}{\sigma^2} ,$$

and with suitable conductivity data one could determine if this equation is obeyed. The phase diagram of the system would make it possible to calculate the conductivity as a function of concentration and temperature from our data on T_D.

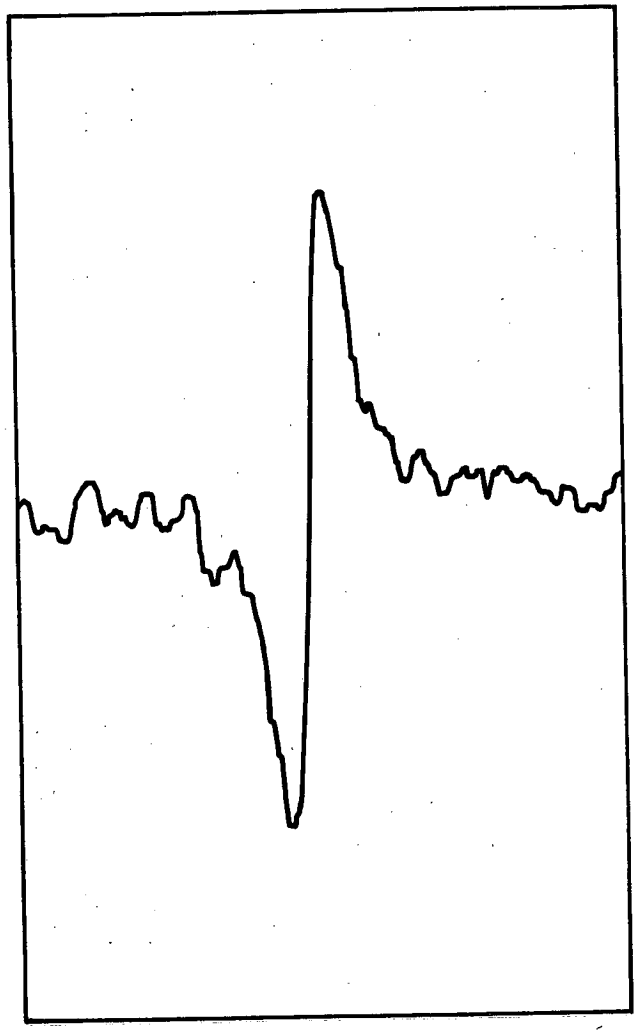

MU-25119

Fig. 7. Li in LiI at room temperature. Sample had previously been heated to 500°C.

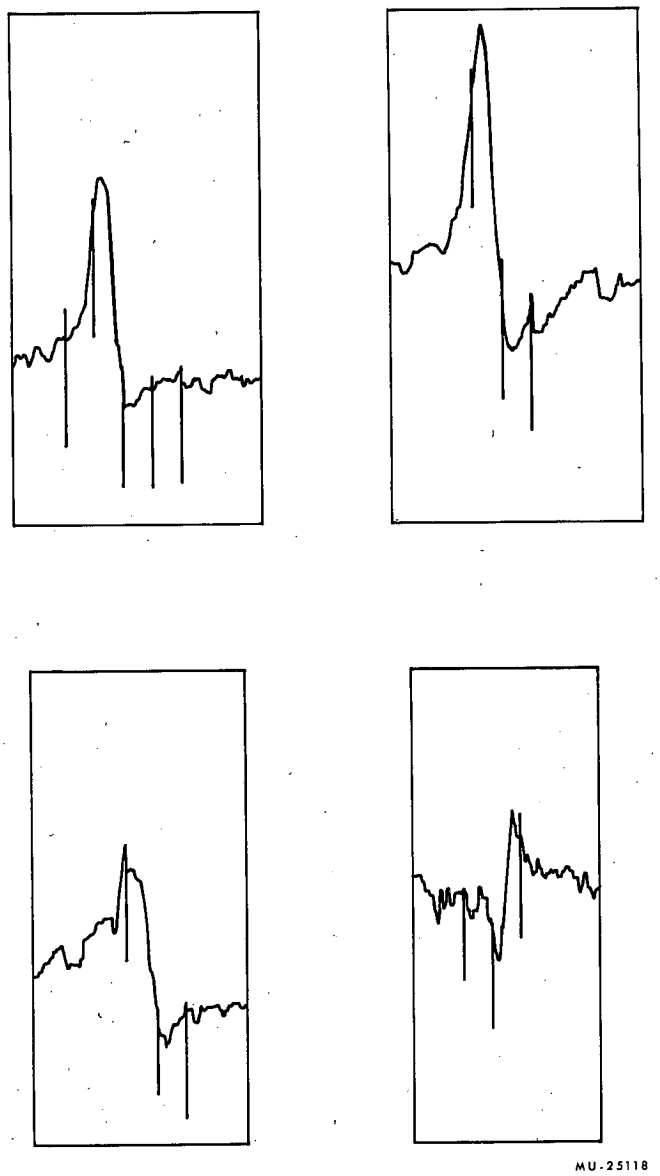

Fig. 8. Li in LiI before solution formation. Interval between frequency markers = 11.7 gauss. Temperatures: above, left, 25°C, right, 170°C; below, left, 266°C, right, 390°C.

The results of the measurements of g values* and relaxation times are found in Table II. The error quoted in each case is the average deviation from the mean. This could be somewhat misleading for the g values, since the field at resonance measured differs from the tru value by the magnitude of the field swept during a time equal to the time constant. Therefore, it would have been more accurate to calculate the deviation from the mean of the average of each two successive measurements. (These involve a reversal of field.) However, the error due to changing the position of the frequency probe during the course of an experiment was neglected and is estimated as ± 0.001. Therefore it is felt that the errors quoted are representative of the experimental accuracy.

It can be seen that the g values are temperature-independent and agree quite well with Feher's more accurate measurement of 2.0023 (± 0.0001), the free-electron value. The relaxation times are somewhat more difficult to interpret. At temperatures up to 280°C there is no real change in T_2 for the samples in which no Li-LiI solution had been previously formed. However, at higher temperatures and for samples which had been heated above the LiI melting point prior to measurements, there is an apparent increase in T_2. In this case there is probably a small amount of LiI dissolved in the lithium metal which could quite conceivably alter the relaxation. However, it is the increase in T_2 which is surprising. According to Elliott's generally accepted theory of relaxation in metals,[18] the relaxation is the result of a scattering mechanism. Thus one would expect the introduction of the salt as an impurity to lead to more effective scattering and a decrease in relaxation time. It would seem that our results call for an alternative explanation. However, it is possible that the heating procedure simply resulted in driving off volatile impurities from the lithium metal. Feher and Kip reported that in the purification of this metal the first distillate had the shortest relaxation time.[13]

At temperatures over the LiI melting point no resonance was observed. An estimate of the relaxation time made from a consideration of the sensitivity of the apparatus determined with other molten salt solutions (see Chapter III), the solubility of lithium metal in lithium iodide (1.2 mole % at 550°C [14]), and the skin depth of the solution estimated from the conductivity of Na-NaBr at the same concentration[6] indicates

$$T_2 < 2 \cdot 10^{-10} \text{ sec.}$$

This value is not at all surprising and could be explained in a number of ways. Experiments on transition-metal ions in molten salt solutions (Cf. Chapter III) indicate that the intrinsic line width is so broad as to be unobservable except for exchange narrowing in concentrated solutions. Therefore it would seem that the relaxation time to be expected in molten salt solutions is small relative to that encountered in media of high dielectric constant. This is probably due to the ionic nature of the solvent and motional effects at the greater temperatures involved. (Cf. p. 2.)

*These values are relative to $g_{DPPH} = 2.0036$.

Table II. Li in LiI.

Sample	Temperature range (°C)	Number of measurements	g	$T_2 \cdot 10^{-9}$ (sec)
1	25 to 100	10	2.001 ± 0.001	6.5 ± 0.8
	100 to 170	12	2.002 ± 0.001	6.8 ± 1.0
	229 to 280	9	2.004 ± 0.002	5.5 ± 0.6
	336 to 447	6	2.003 ± 0.002	
		9		8.4 ± 1.5
	25	5	2.002 ± 0.001	
		7		8.7 ± 0.7
	29 to 100	5	2.002 ± 0.001	
		9		8.2 ± 0.4
	100 to 206	7	2.002 ± 0.001	
		6		8.8 ± 1.2
	25	3		8.2 ± 0.5
2	25	4	2.003 ± 0.001	6.8 ± 0.1

II. TEMPERATURE EFFECTS IN ULTRAVIOLET-IRRADIATED LITHIUM HYDRIDE

A. Introduction

This experiment was conducted primarily to test the apparatus described on page 7 ff. Also, it was hoped that the study of colloidal lithium metal would be of value in the subsequent study of Li in LiI.

In 1959, Ingram et al. discovered an extremely narrow ESR line (0.1 gauss) in uv-irradiated LiH, which was attributed to colloidal lithium metal on the basis of constant intensity of the line at room temperature and 90°K.[15] This is expected in a metal, since the population at the Fermi surface is proportional to T while the excess population of the lower spin state varies as 1/T. The properties of irradiated LiH have since been studied extensively by Pretzel and co-workers.[16]

An earlier study of ESR line width vs temperature had indicated that when a metal was heated over its melting point, there was a discontinuity;[17] e.g., for lithium metal above and below 186°C the line width was found to be 3.1 gauss and 1.9 gauss, respectively, for the full width at half maximum. This was predicted by Elliott's theory of spin-orbit coupling effects in magnetic resonance of conduction electrons,[18] according to which $\Delta H \propto (\Delta g)^2 \rho$. Here Δg is the g shift and ρ the resistivity of the metal, which is, of course, discontinuous at the melting point.

On the basis of these two experiments it was felt that it would be interesting to determine whether the discontinuity in line width could be observed on heating an irradiated LiH sample above the melting point of lithium metal. This would corroborate the existence of colloidal lithium metal.

B. Experimental Method

Powdered lithium hydride obtained from the Maybeck Chemical Company was sealed in quartz capillaries in a vacuum of approximately 10^{-5} mm Hg. The sample was then irradiated for 30 minutes with the 2537 A line from a mercury lamp. ESR measurements were made with the apparatus described on p. 7 and the spectrometer of p. 12.

C. Experimental Results and Discussion

The intensity of the line was found to be drastically reduced at 95°C and the line had disappeared completely at a temperature of 170°C. At the same time the original black color of the sample had bleached out to white.

These results are somewhat surprising in view of Pretzel's observation that the intensity of the lithium colloid band increases markedly in the optical region after a 19-hour thermal bleach at 27 to 72°C. See Fig. 7 of Ref. 19. The history of this sample was, of course, quite different from ours, having been repeatedly x-irradiated. Even so, the apparent paradox

is unresolved unless the higher-energy irradiation yields larger and, therefore, more stable colloidal centers.

Apart from this disparity with Pretzel's results, the bleaching that was encountered at elevated temperatures might not have been totally unexpected. F centers formed by irradiation are known to bleach out upon heating.[20] This is presumably due to mutual annihilation of electrons and holes, and could be applicable to our case. However, it might be necessary to postulate an intermediate step, such as diffusion of lithium colloid to form interstitial lithium atoms or F centers.

III. TEMPERATURE EFFECTS IN MOLTEN SALT SOLUTIONS AND POWDERS CONTAINING TRANSITION-METAL IONS

A. Introduction

Molten salt solutions have been investigated by a wide variety of techniques, including more recently the tools of spectroscopy.[21] Spectroscopic techniques usually give more detailed information regarding the exact state of the species studied, as they involve direct measurement of microscopic properties. Thus the additional information obtained from any new type of spectroscopic measurement is of fundamental importance.

The present work in electron spin resonance of paramagnetic ions in molten $ZnCl_2$ and in LiCl-KCl eutectic (chosen for its relatively low melting point) is of twofold interest. First, the measurement of g values should give an indication of the species present. For example, a marked change in g value as a function of concentration or temperature would imply a change in complex formation. An the line width in some cases is an indication of the environment of the ion. Second, these solutions offer a vastly different medium from any heretofore investigated for relaxation studies. The viscosity, especially in the case of $ZnCl_2$, is much greater than that for water solutions, and the ionic nature of the solvent would make a priori an entirely new relaxation mechanism conceivable.

It is hoped that the author's greater interest in the relaxation phenomenon and consequent emphasis thereupon will not obscure the relevance of the results for those more interested in the chemistry of molten salt solutions.

The temperature effects encountered in the solids were somewhat incidental with respect to the general scope of this work. However, some interesting effects were observed which are discussed and compared with previous results in Part D.

A fairly complete discussion of the literature on relaxation in liquids has been given recently by R. G. Hayes.[22] Therefore, we shall for the most part only briefly recapitulate the theories which have relevance to our work.

It was first shown by the work of Bloembergen, Purcell, and Pound[3] that the Brownian motion in a liquid averages out the dipolar Hamiltonian, giving rise to a much narrower nuclear resonance line width than that found in solids. This averaging procedure was later employed by McConnell[23] with a slightly different mechanism. In his "microcrystallite theory" McConnell assumed that a transition-metal ion is surrounded by ligands in such a manner as to give rise to magnetic anisotropies in the first coordination sphere. It is thus the averaging of these anisotropies which determines the relaxation.

McGarvey[24] extended the McConnell theory to systems possessing zero-field splittings and thus attempted to interpret his observed line widths in Cr^{+3}, Mn^{+2}, and Fe^{+3} in aqueous solutions.

The effect of the exchange interaction[25] was included by Kivelson[26] in a rather sophisticated treatment. This calculation is essentially a derivation of the McConnell parameters using the formalism developed by Kubo and Tomita.[27] Included are the effects of the nuclear quadrupole moments, zero-field splittings, anisotropic Zeeman terms, electronic-electronic and nuclear-electronic dipolar interactions, Fermi contact interaction, and motional Hamiltonian, as well as the exchange forces. He neglected the effect of spin-orbit coupling.

Russian workers[28] have considered the adaptation of the Van Vleck mechanism[29] as an explanation of relaxation in liquids. This would involve an electron spin-phonon interaction via the spin-orbit coupling. However, the validity of their calculations is questionable, according to Hayes.[22]

Finally, Bloembergen and Morgan have concluded that electron spin relaxation is determined by a collision mechanism resulting in the distortion of the solvated transition-metal ion complex.[30] Here it is principally by means of the spin-orbit coupling that relaxation occurs.

It can be concluded from these papers that there is no unified treatment of relaxation which can be applied to a variety of ions even in aqueous solution, and the applicability of any of these theories to molten salt solutions remains to be tested by experiment. In a later section our experimental results are compared with several of these theoretical predictions.

B. Experimental Method

1. Sample Preparation

The solid compounds were weighed on a torsion balance and ground together with a mortar and pestle; they were then placed in 5-mm i.d. glass tubes and heated at 200°C in vacuum until a pressure of less than 10^{-4} mm of mercury was reached (6 to 12 hours). At this point the heater was removed and the tube sealed approximately 2 cm from the end, the sample occupying about 1 cm of this length. Some of the samples were then melted at 400°C prior to measurements.

All chemicals were reagent grade and were obtained from the following companies:

$MnCl_2$	K and K Laboratories, Inc.
LiCl	Merck and Company, Inc.
KCl	Allied Chemical Company
$CrCl_3$	Fisher Scientific Company
$MnCl_2 \cdot 4M_2O$	Allied Chemical Company
$NiCl_2 \cdot 6H_2O$	Allied Chemical Company
$FeCl_3$	Matheson, Coleman and Bell
$VOCl_2$	United Mineral and Chemical Company

The hydrated $NiCl_2$ was heated at 200°C in vacuum to give $NiCl_2$. An x-ray analysis of the dried $MnCl_2$ powder indicated that no hydrate was present.

The $VOCl_2$ was in the liquid state as received from the manufacturer. It was dried in vacuum to give a blue-black solid which was then mixed with LiCl-KCl and dried as described above. Some of the solid was dissolved in water, and the ESR spectrum of the solution was taken to test this starting material. We did indeed find the characteristic VO^{++} spectrum; but we still cannot be absolutely certain that the solid compound was anhydrous $VOCl_2$.

2. Measurement of Line Widths

All measurements were made with the terminated-wave-guide apparatus and the spectrometer described in Chapter I, Part B. This apparatus required approximately 45 minutes to come to thermal equilibrium; consequently, the line widths were usually measured while heating with temperature increments of 5° to 10°C during a single measurement. Temperatures quoted are averages of initial and final sample temperatures.

The sample temperature as a function of temperature measured was calibrated by means of two thermocouples, one in the usual position (see Fig. 5) and the other in a sample tube with LiCl-KCl eutectic mixture in the usual sample position. This temperature difference was appreciable (~ 100°C) at the higher temperatures, and, therefore, an upper limit of ± 5°C is set upon the temperatures reported. There was not this great a variation within the calibration curves, but the potentiometer itself introduces an additional uncertainty, which is included in the above error, as well as the temperature increment during measurement.

C. Experimental Results

The experimental results for paramagnetic ions in both the powders and liquids are found in Figs. 9 through 29 and Table III, which summarizes the results in solids. See also Table IV for values of hyperfine-coupling constants and hyperfine component line widths of the $MnCl_2$-LiCl-KCl system. Figures 21 through 29 are reproductions of observed spectra, while Figs. 9 through 20 are graphs of line width measurements. The melting points are not marked on these graphs as they are not accurately known. The melting points of the mixtures are slightly lower than those of the pure solvents, which are

$$T_M = 318^\circ C \text{ for } ZnCl_2,$$

$$T_M = 352^\circ C \text{ for LiCl-KCl.}$$

The concentrations are given both in mole percent, as is conventional for solids, and in approximate volume molarity. These values were calculated by using $\rho_{LiCl\text{-}KCl} = 1.885$ g/cc,[31] and $\rho_{ZnCl_2} = 2.481$ g/cc.[32] Line widths represent the full width between points of maximum slope on the absorption curve. The errors can be estimated from the scatter of points in Figs. 9 to 20. The line widths for the solids are believed to be good to ±10%; however, the results in liquids are good only to ±15% at best. This is due to

the difficulty in determining the maximum for broad lines, the asymmetric line shape which makes the determination of one of the maxima even more difficult, and the limited signal-to-noise ratio. The scatter of points encountered in a few of the graphs of solids at elevated temperatures is due to an unbalance of the microwave bridge which was caused by an excess temperature increment during the time of measurement.

1. $MnCl_2$ in LiCl-KCl (Figs. 9 to 12 and 21 to 25)

The line width is very much dependent upon the sample history. If the sample was simply dried before measurement, a sharp line (approx 26 gauss) was obtained for all concentrations. That this line was due to the drying procedure was ascertained by a line-width measurement of a sample not subjected to this procedure. (See Tables III and IV.) On the other hand, if the sample was dried and then melted before measurement, a relatively broad line (approx 170 gauss) was found. Only the 0.3 mole % sample showed clearly defined hyperfine structure at room temperature in addition to the usual narrow and sharp lines.* The disappearance of the latter lines upon heating may be seen in Fig. 21. For the sample which had not been melted, the center line had entirely disappeared at 300°C (not shown). Figures 22 to 24 show the appearance of hyperfine structure as a function of temperature for all concentrations, and are largely self-explanatory.

No resonance was observed in the 0.3 mole % sample in the liquid state. The line width can be estimated from Fig. 11 to give a value of $C/\Delta H^2 > 10^{-6}$ for the limiting sensitivity; C is the molar concentration and ΔH the line width in gauss. The 6.1 mole % sample gave a single line at all temperatures and is not included. In Fig. 25 may be found examples of the line shapes encountered in the liquids. See discussion in the Appendix. The latter two measurements were of samples in 2-mm i.d. tubes rather than the usual 5-mm ones, and the line shapes are accordingly found to be more symmetric. Unfortunately, the smaller sample size also led to a poorer signal-to-noise ratio and even poorer line-width measurements.† Therefore, these measurements are not included in Fig. 10, but are shown here in an attempt to justify the large experimental error quoted for the liquids. The asymmetry was found to increase with increasing $MnCl_2$ concentration. Cf. Fig. 22. This point will not be commented upon further.

A summary of the experimental line widths for all concentrations and temperatures may be found in Fig. 12. Notice the decreasing line width as a function of concentration. A comparison of line width vs concentration for

---

*There is very faintly perceptible hyperfine structure in the 0.9 and 1.4 mole % samples.

†Experiments with various sample sizes for concentrated Mn^{++} in H_2O indicated that the line widths were the same for symmetric and asymmetric line shapes. It was simply more difficult to determine the maximum in the asymmetric case for equal signal to noise. Theory predicts a difference of 10%.

$MnCl_2$ in LiCl-KCl at 400°C and Mn^{++} ($MnCl_2$) in water is given in Fig. 11. Also included is Fig. 26, which shows the difference in the appearance of hyperfine structure upon dilution in the Mn^{++}-water system and upon heating the solid $MnCl_2$-LiCl-KCl system.

2. $MnCl_2$ in $ZnCl_2$ (Figs. 13, 14, 27 and 28)

No hyperfine structure was observed at any concentration or temperature studied. The increasing asymmetry of the line with increasing concentration and temperature can be seen in Figs. 27 and 28. The line width measurements are summarized in Fig. 14. It would appear that the line widths in the liquid decrease with increasing concentration; however, the measurements are insufficiently accurate for certainty. This decrease, if it is real, is only about 6%.

3. $MnCl_2$ in $MnCl_2 \cdot 4H_2O$ (Fig. 15)

At 105°C, $MnCl_2 \cdot 4H_2O$ loses two of its waters of hydration and there is apparently a slight increase in line width with temperature beginning at this point. Here again, the data are insufficiently accurate for certainty.

The g value of Mn^{++} in the solids was found to be 2.00. In the liquids we found $g = 2.03 \pm 0.02$ for 1 M $MnCl_2$ in LiCl-KCl and $g = 2.013 \pm 0.004$ for 2 M $MnCl_2$ in LiCl-KCl; there was no temperature variation. The g values were not measured for the $MnCl_2$ - $ZnCl_2$ solutions.

4. $CrCl_3$ and $CrCl_3$ in LiCl-KCl and in $ZnCl_2$ (Figs. 29 and 16 to 18)

A summary of these data is found in Fig. 18. Figure 29 demonstrates the increase in line width with temperature that was observed in sublimed $CrCl_3$ and the line shapes encountered in the spectra of the liquids.

The g value of $CrCl_3$ increases gradually from a room-temperature value of 1.975 ± 0.005 to 2.000 ± 0.005 at temperatures in the neighborhood of 325°C. In 5.5 mole% $CrCl_3$ in $ZnCl_2$, there is a very slight decrease in g value from 1.988 ± 0.002 at room temperature to 1.983 ± 0.002 at 280°C. In the liquid state there is again an apparent decrease from $g = 2.006 \pm 0.002$ at 340°C to $g = 1.993 \pm 0.002$ at 375°C. These values were determined by the method described in the Appendix. There was no variation in g values for $CrCl_3$ in LiCl-KCl in the liquid or solid. These were found to be $g = 1.985 \pm 0.002$ (solid) and $g = 2.006 \pm 0.003$ (liquid).

5. $NiCl_2$ in LiCl-KCl, $FeCl_3$ in LiCl-KCl, and $VOCl_2$ in LiCl-KCl (Figs. 19-20)

No resonance was observed in the liquid state for any of these samples. The $NiCl_2$-LiCl-KCl system (see Fig. 19) gave the largest temperature variation of line width (1090 gauss to 590 gauss) encountered in this work; this was accompanied by a decrease in g value from 2.35 ± 0.03 to 2.23 ± 0.01.

An attempt was made to observe the $FeCl_3$ resonance in the gaseous state by heating the sealed tube of $FeCl_3$ over the boiling point (315°C); no resonance was observed.

Table III. Summary of Results in Solids

Compound	Concentration		ΔH at room temperature (gauss)	Qualitative behavior on heating
	Molarity	Mole %		
$MnCl_2$ in LiCl-KCl	0.1	0.3	Central line 28; hyperfine component 20	Central line disappears
	0.1 (m)	0.3	Broad background line ≈ 200 gauss; hyperfine component 20	Background line disappears
	0.3, 0.5, 1	0.9, 1.4, 2.8	28	Appearance of hyperfine structure
	0.3, 0.5, 1(m)	0.9, 1.4, 2.8	170	Appearance of hyperfine structure
	2	6.1	26	No change
$MnCl_2$ in LiCl-KCl (not dried)	1	2.8	456	
$MnCl_2$ in KCl	1	3.8	23	
$MnCl_2$ in LiCl	1	2.1	21	
$MnCl_2$ in $ZnCl_2$	0.5	2.74	570	Slight decrease of ΔH
	1	5.4	675	Decrease of ΔH
	1(m)	5.4	475	
$MnCl_2$			860	Decrease of ΔH
$MnCl_2 \cdot 4H_2O$			485	Only slight change
$CrCl_3$ in LiCl-KCl	0.5(m)	1.5	137	No change
	1(m)	2.8	120	No change
$CrCl_3$ in $ZnCl_2$	1(m)	5.5	72	No change
$CrCl_3$			77	Increase of ΔH beginning at 240°C
$NiCl_2$ in LiCl-KCl	1(m)	3.0	1090	Decrease of g values and almost linear decrease of ΔH
$FeCl_3$ in LiCl-KCl			110	Rapid increase of ΔH at 240°C
$FeCl_3$			435	Slight decrease of ΔH
$VOCl_2$ in LiCl-KCl	1	2.9	29	No change
	1 (m)	2.9	29	No change

(m) indicates that the sample had been melted prior to measurement. There are no comments in the last column for cases in which no heating experiments were performed.

Table IV. Line widths of hyperfine components and coupling constants of $MnCl_2$ in LiCl-KCl

Mole % Mn^{++}	No. of measurements	Temp. range (°C)	ΔH (M_I)						$A(M_I, M'_I)$				
			$-\frac{5}{2}$	$-\frac{3}{2}$	$-\frac{1}{2}$	$\frac{1}{2}$	$\frac{3}{2}$	$\frac{5}{2}$	$-\frac{5}{2}, -\frac{3}{2}$	$-\frac{3}{2}, -\frac{1}{2}$	$-\frac{1}{2}, \frac{1}{2}$	$\frac{1}{2}, \frac{3}{2}$	$\frac{3}{2}, \frac{5}{2}$
0.30	17	25-235	22	21	21	20	20	21	83	84	87	90	93
0.30	20	25-317	22	21	20	18	20	22	82	84	85	90	92
0.89	12	194-280	22	19	17		17	20	82	82			94
1.1	6	270-307	22	19	22	20	20	20	84	85	86	87	93
1.1	6	180-283	29	28	31	27	25	26	79	82	82	86	89
2.8	17	186-289							81			87	94
2.8	2	298-306	20	16	16	16	18	19	81	82	81	85	93
2.8	4	306	25	30	33	26	22	26	83	84	85	88	91

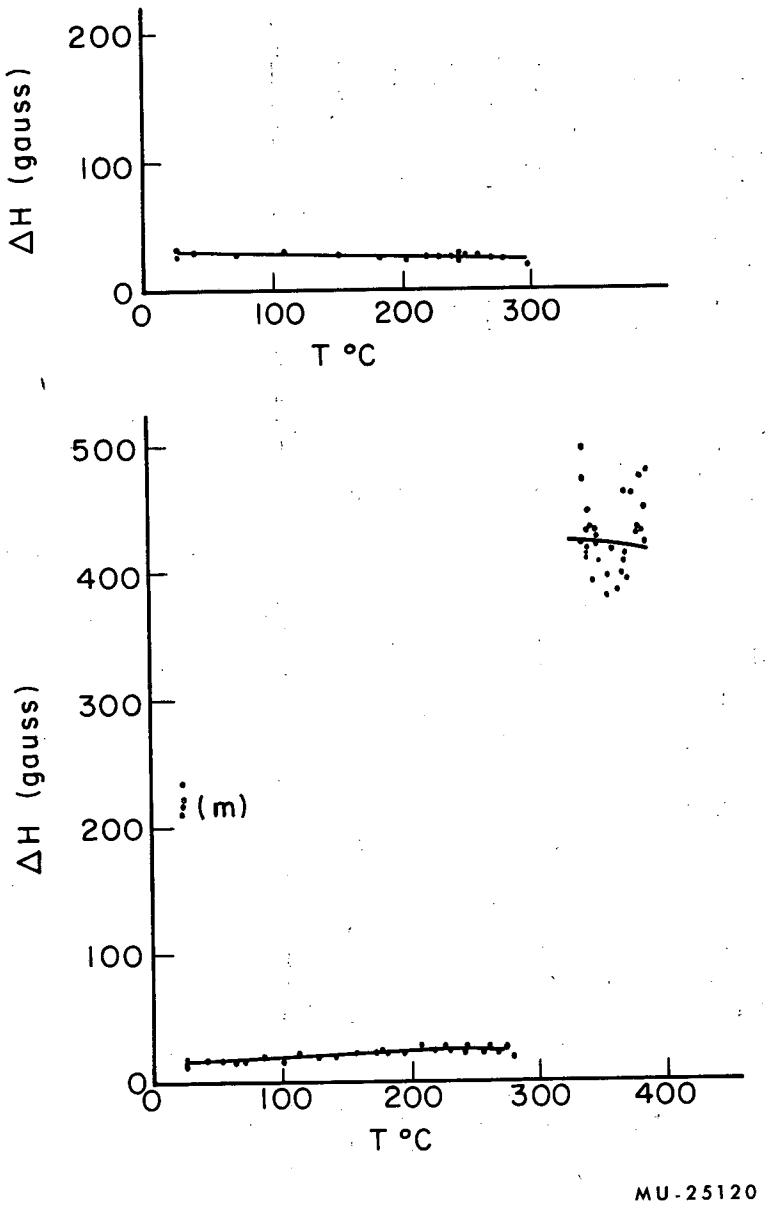

Fig. 9. $MnCl_2$ in LiCl-KCl.
Above: 0.3 mole% (0.1 M).
Below: 0.9 mole% (0.3 M).

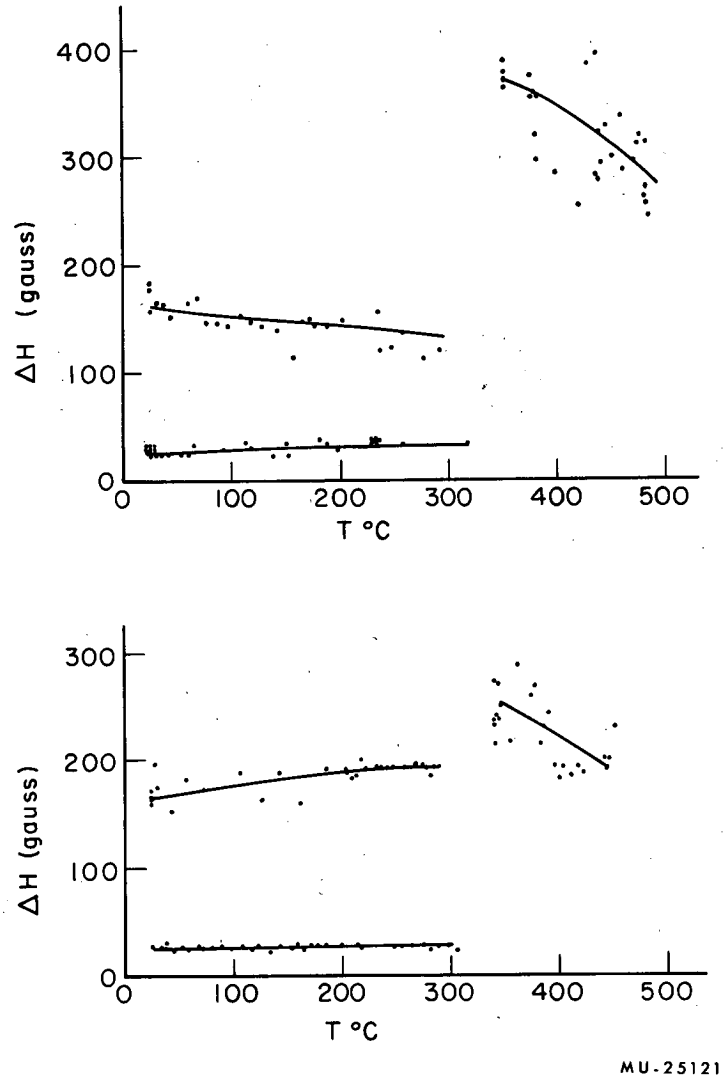

Fig. 10. $MnCl_2$ in LiCl-KCl.
Above: 1.4 mole% (0.5 M).
Below: 2.8 mole% (1.0 M).

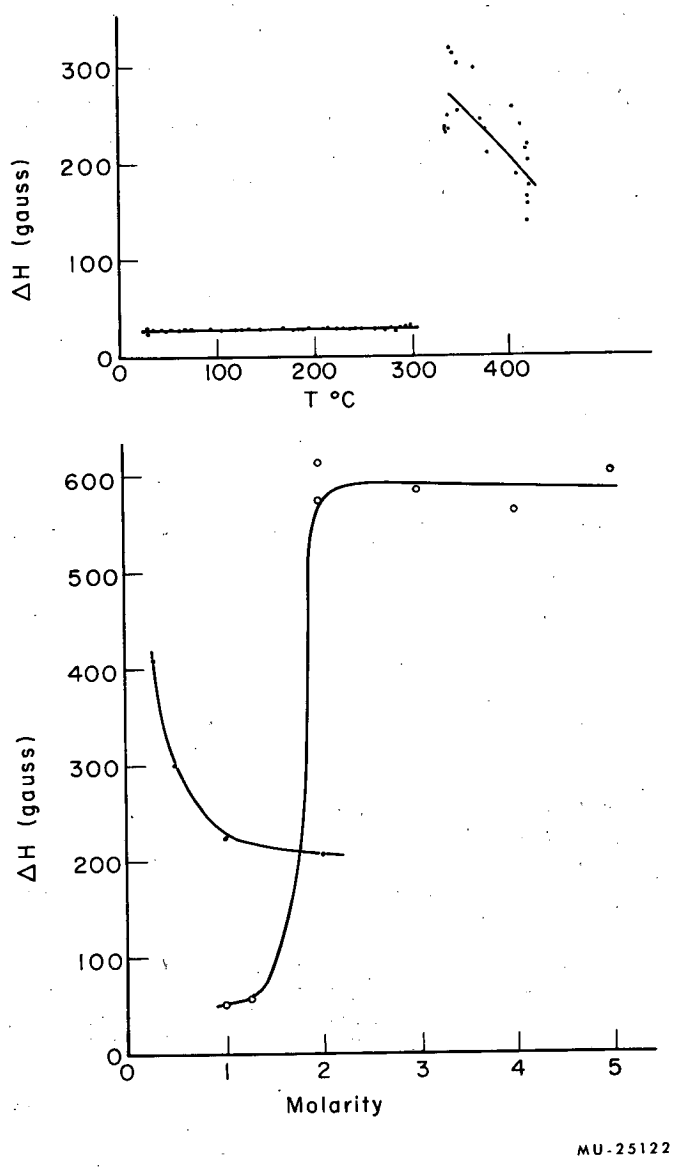

Fig. 11. $MnCl_2$ in LiCl-KCl and a comparison of the $MnCl_2$-LiCl-KCl and Mn^{++}-H_2O systems as a function of concentration.
Above: 6.1 mole% (2 M).
Below: • $MnCl_2$ in LiCl-KCl at 400° C,
° Mn^{++} in H_2O at 25°C.

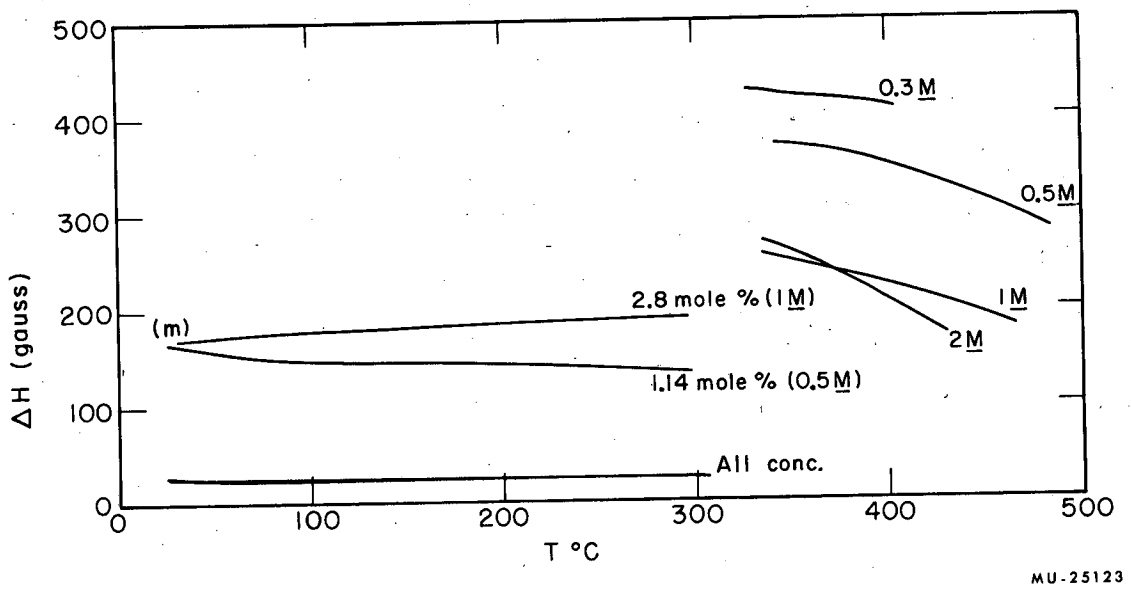

Fig. 12. Summary of line widths of $MnCl_2$ in LiCl-KCl.

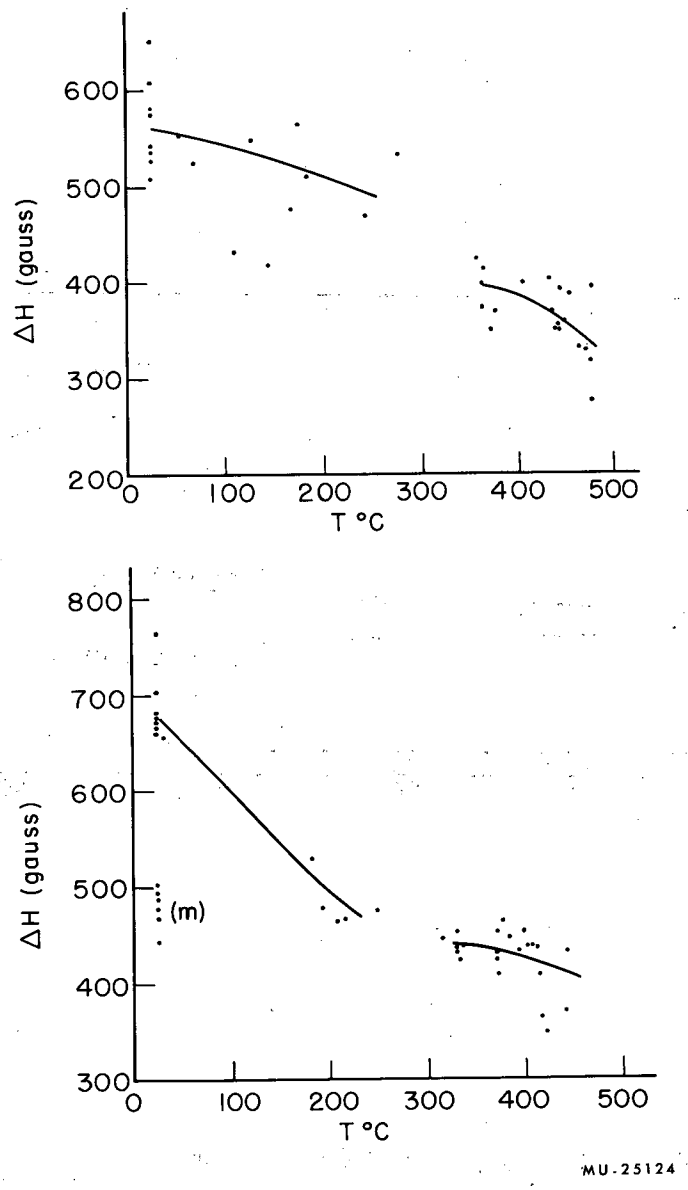

Fig. 13. $MnCl_2$ in $ZnCl_2$.
Above: 2.7 mole% (0.5 M).
Below: 5.4 mole% (1 M).

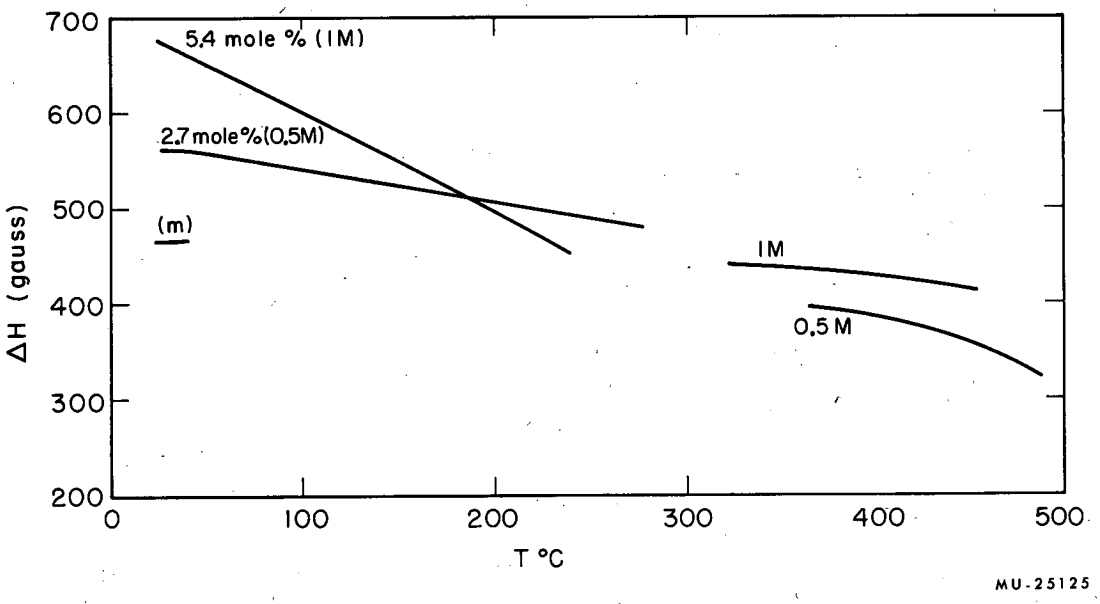

Fig. 14. Summary of line widths of $MnCl_2$ in $ZnCl_2$.

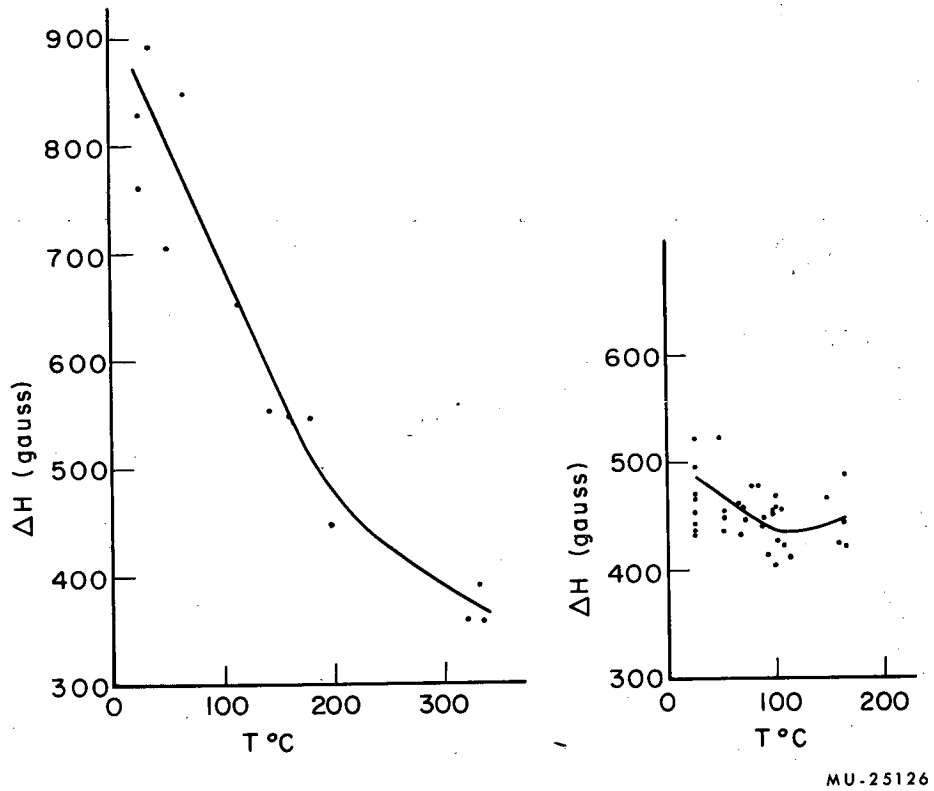

Fig. 15. $MnCl_2$ (left) and $MnCl_2$-$4H_2O$ (right).

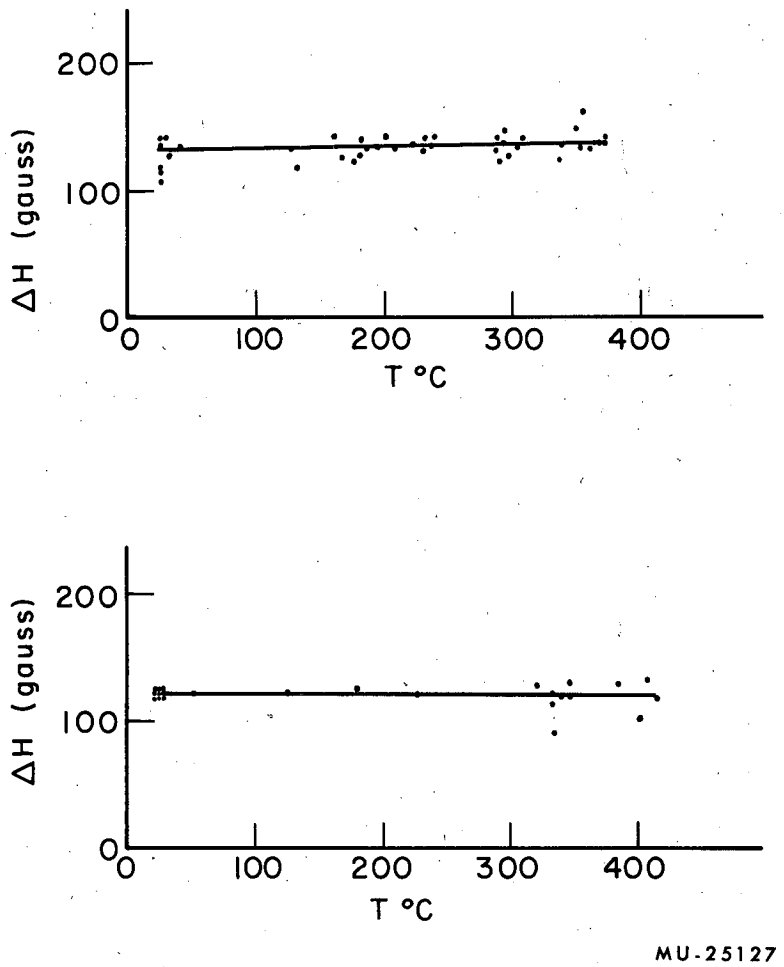

Fig. 16. $CrCl_3$ in LiCl-KCl.
Above: 1.5 mole% (0.5 M).
Below: 2.8 mole% (1.0 M).

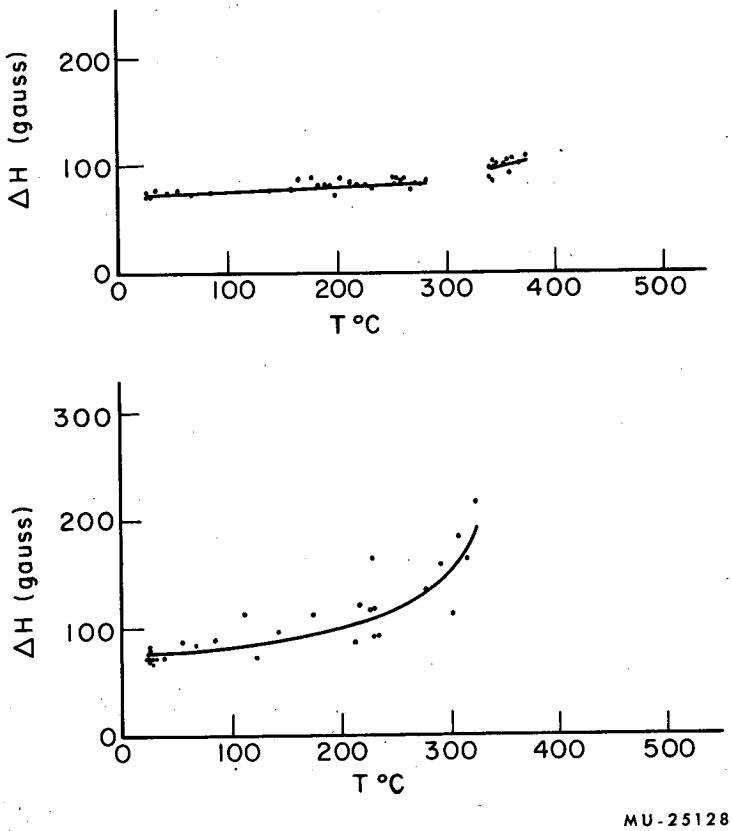

Fig. 17. Above: $CrCl_3$ in $ZnCl_2$, 5.5 mole% (1 M).
Below: $CrCl_3$.

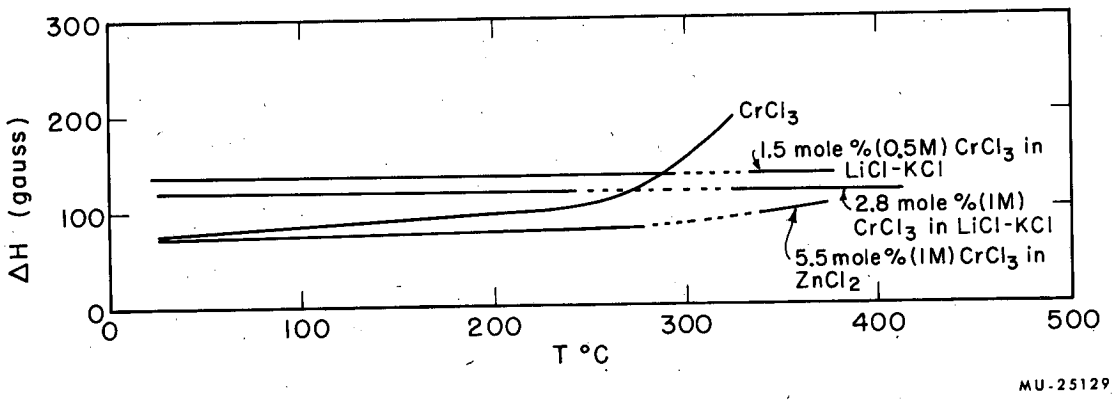

Fig. 18. Summary of Cr(III) measurements.

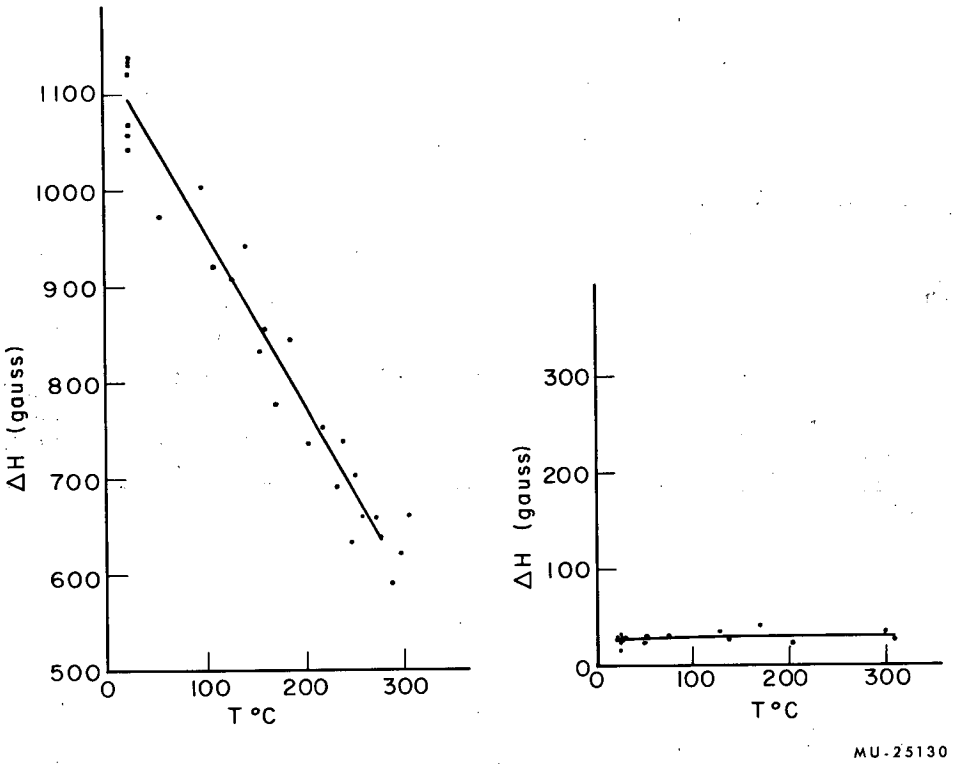

Fig. 19. Left: $NiCl_2$ in LiCl-KCl, 3.0 mole% (1 M).
Right: $VOCl_2$ in LiCl-KCl, 2.9 mole% (1 M).

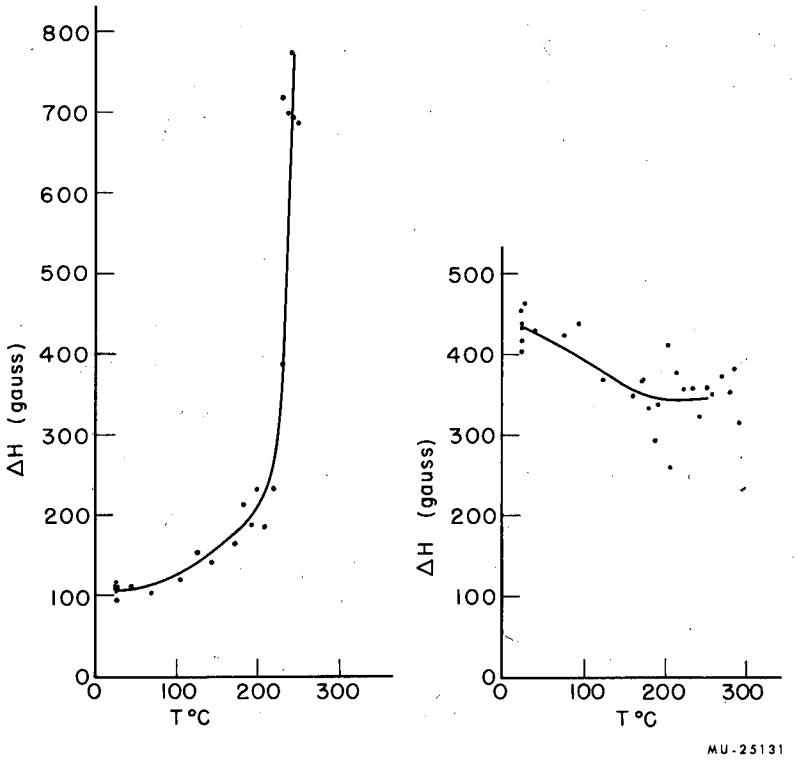

Fig. 20. Left: $FeCl_3$ in LiCl-KCl.
Right: $FeCl_3$.

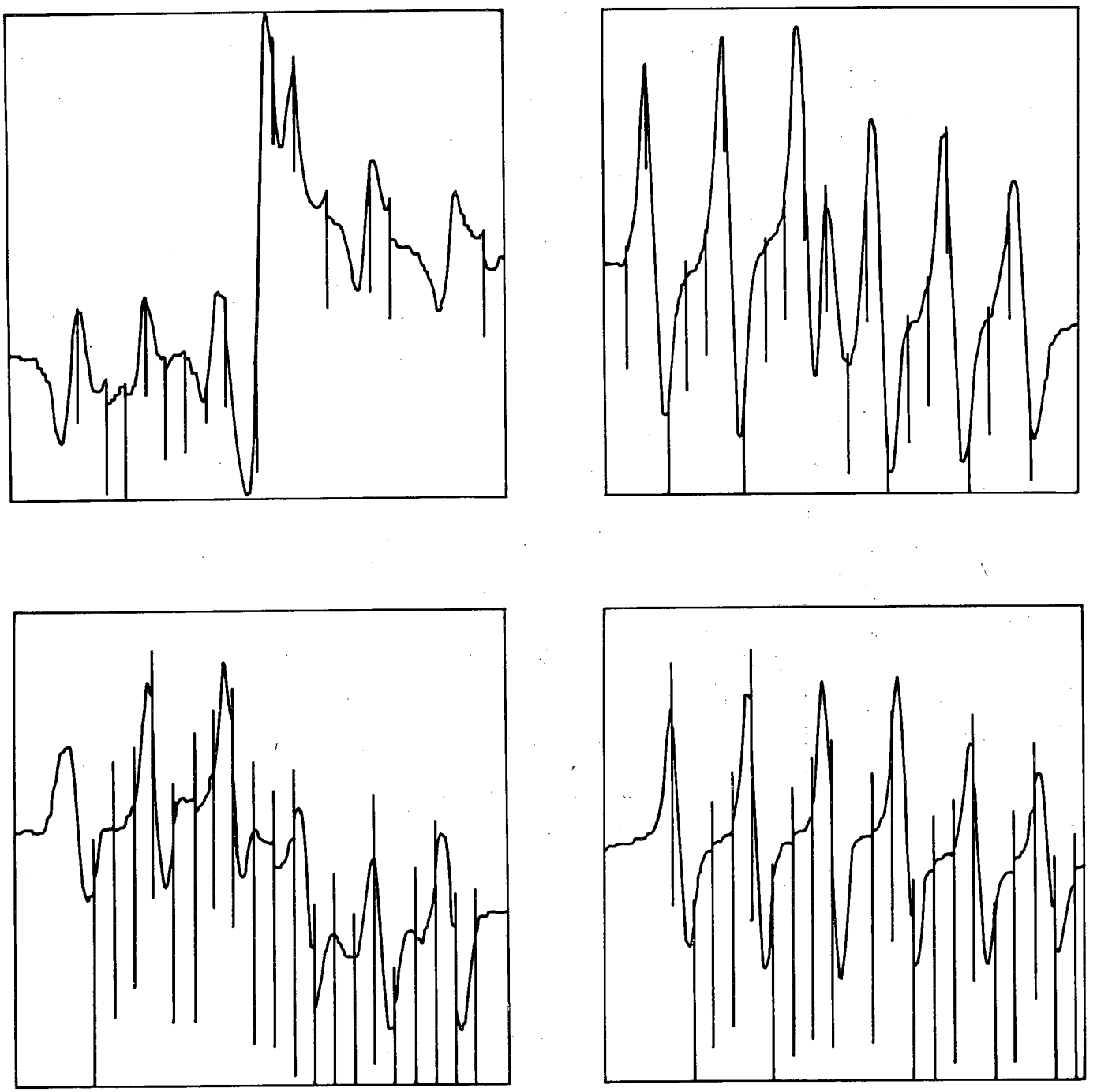

MUB-860

Fig. 21. $MnCl_2$ in LiCl-KCl, 0.3 mole% (0.1 M).
Distance between frequency markers = 23.5 gauss.
Above: left, ΔH = 31 gauss, T = 25°C;
right, ΔH = 23 gauss, T = 277°C.
Below: left, (m), T = 35°C; right, (m), T = 242°C.

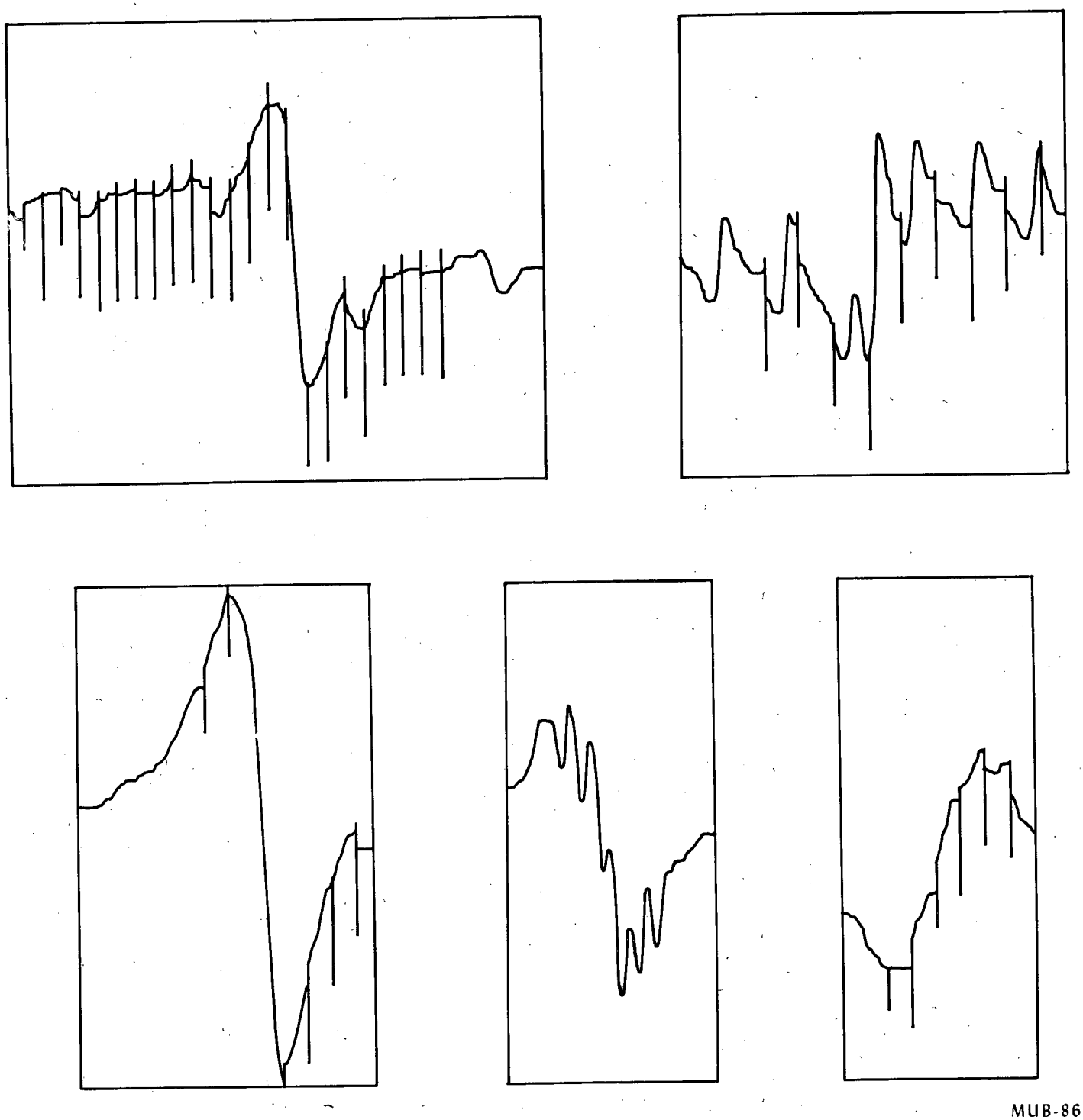

MUB-861

Fig. 22. $MnCl_2$ in LiCl-KCl, 0.89 mole% (0.3 M). Above: left, ΔH = 21 gauss; T = 194°C. 11.7 gauss between frequency markers. right, ΔH = 19 gauss; T = 280°C. 47.0 gauss between frequency markers. Below: left, (m); ΔH = 235 gauss. T = 25°C. 117.5 gauss between frequency markers. center, (m); T = 307°C. right, ΔH = 450 gauss. T = 385°C. 117.5 gauss between frequency markers.

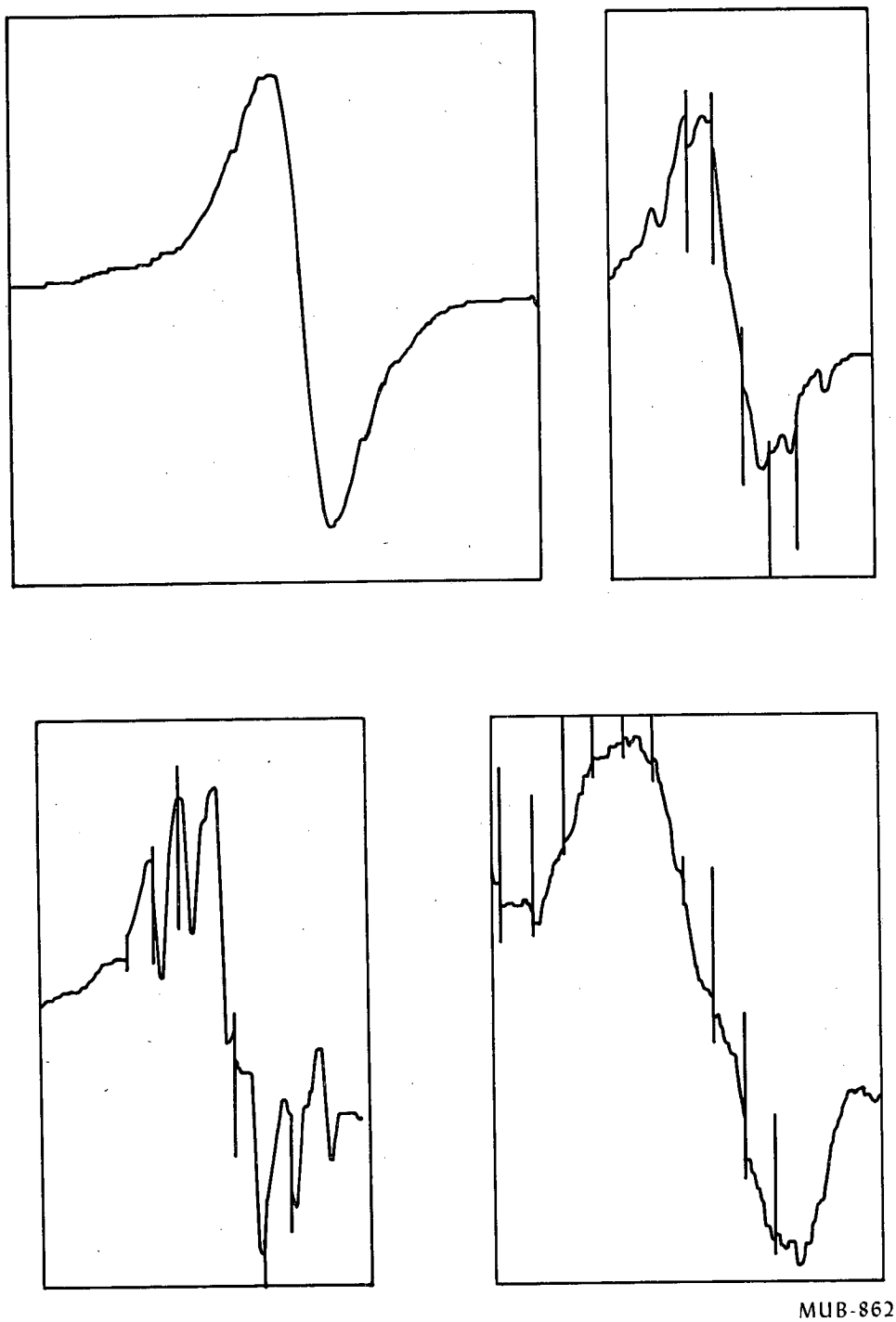

Fig. 23. $MnCl_2$ in LiCl-KCl, 1.1 mole% (0.5 M). Distance between frequency markers = 70.5 gauss. Above: left, (m); ΔH = 155 gauss; T = 25°C; right, (m); ΔH = 146 gauss; T = 118°C. Below: left, (m); ΔH = 113 gauss; T = 277°C; right, ΔH = 390 gauss; T = 352°C.

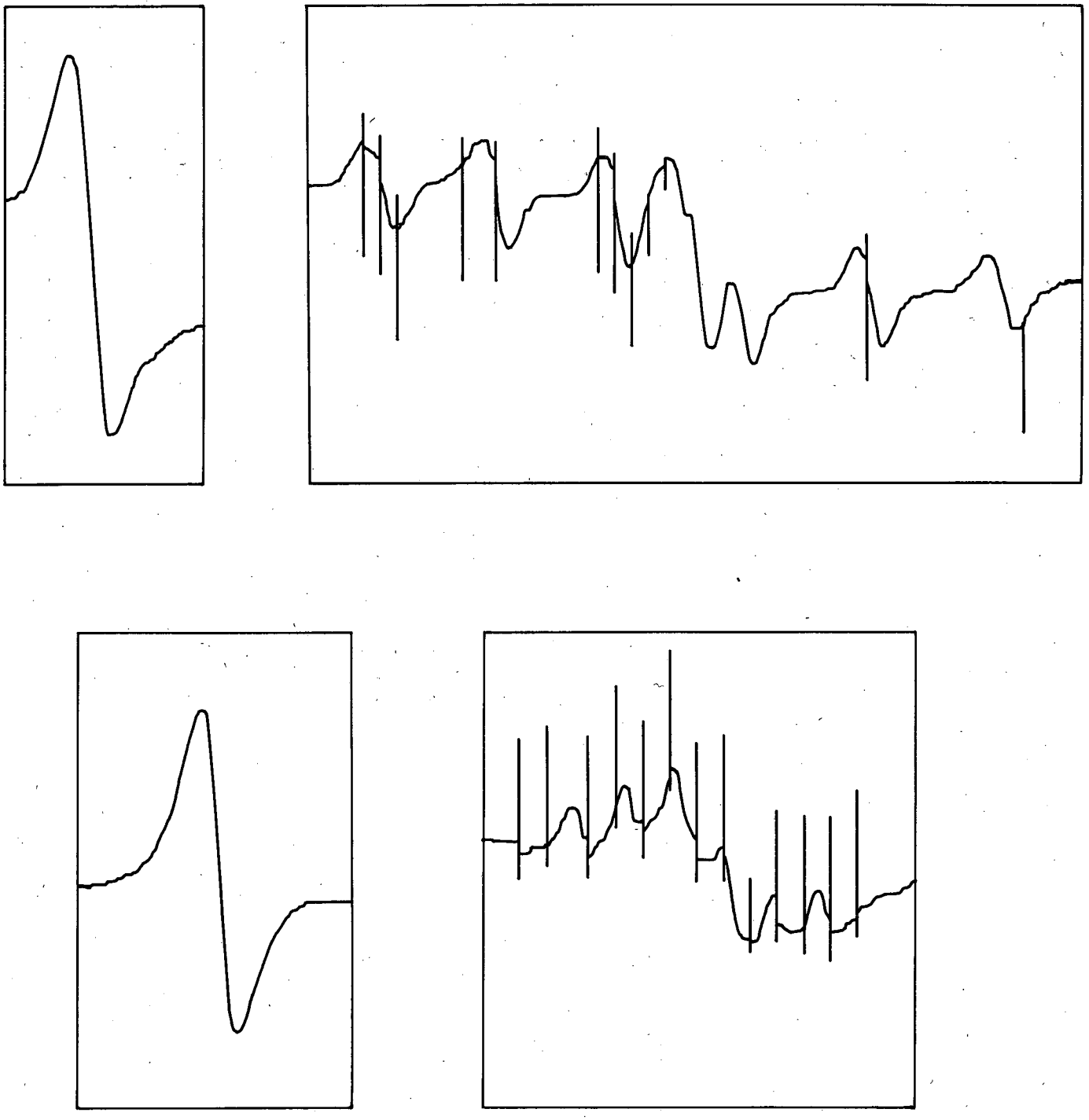

MUB-864

Fig. 24. $MnCl_2$ in LiCl-KCl, 2.8 mole% (1 M).
Above: left, ΔH = 26 gauss; T = 25°C; right, ΔH (center) = 28 gauss; T = 298°C.
Below: left, (m); ΔH = 159 gauss; T = 25°C; right, ΔH = 132 gauss; T = 290°C; 47.0 gauss between frequency markers.

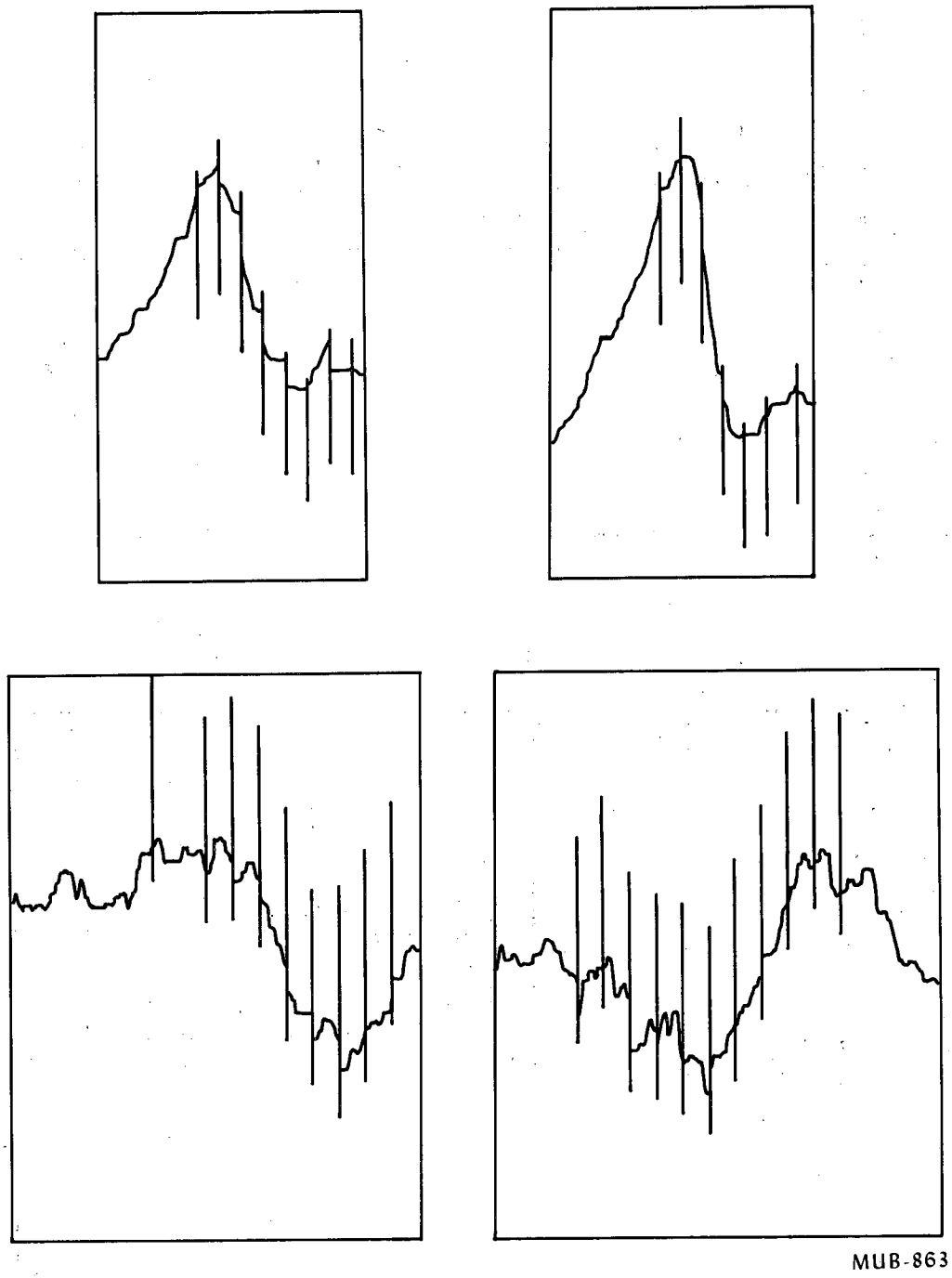

Fig. 25. $MnCl_2$ in LiCl-KCl, 2.8 mole% (1 M).
Interval between frequency markers = 70.5 gauss.
Samples contained in 2-mm i. d. tubes in lower spectra.
Above: left, ΔH = 267 gauss; T = 379°C; ΔH = 194 gauss;
T = 418°C. Below: left, ΔH = 350 gauss; T = 421°C;
right, ΔH = 300 gauss; T = 495°C.

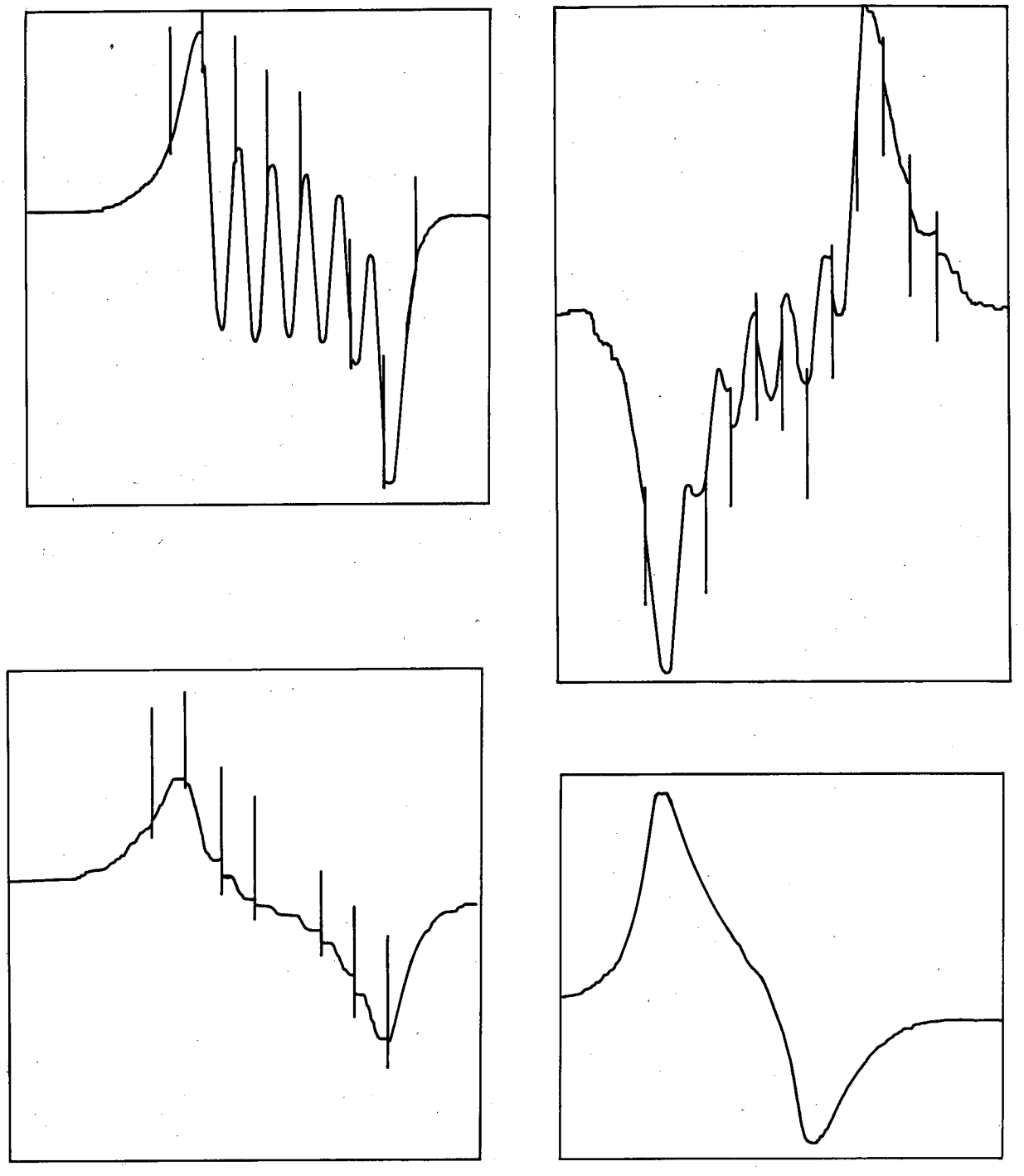

MUB-865

Fig. 26. Mn^{++} ($MnCl_2$) in H_2O. Above: left, 1 M; right, 1.25 M. Below: left, 1.5 M; right, 2 M.

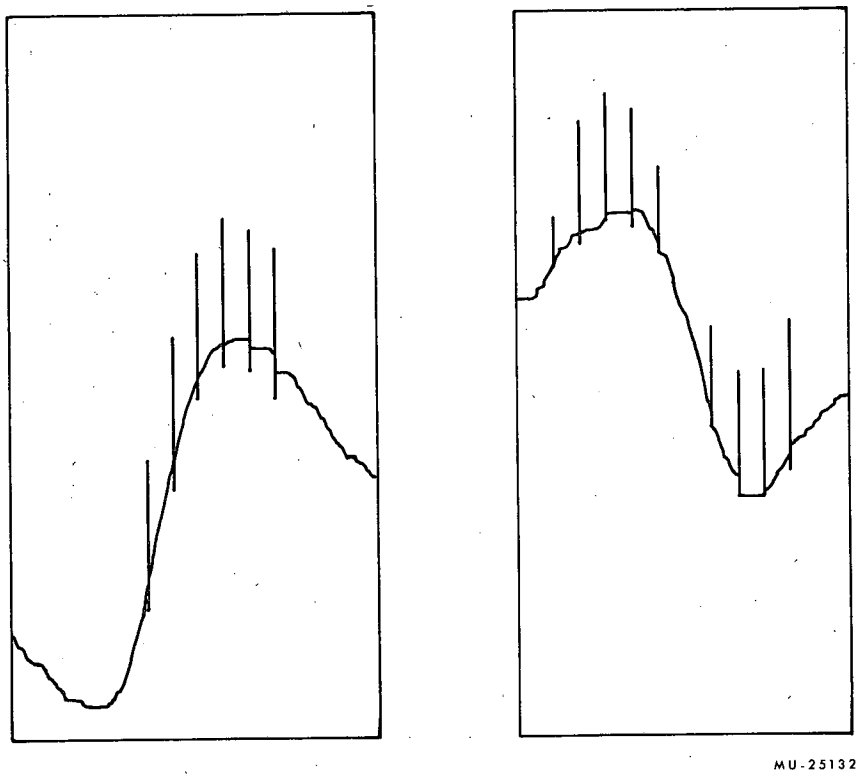

Fig. 27. $MnCl_2$ in $ZnCl_2$, 2.7 mole% (0.5 M). Interval between frequency markers = 70.5 gauss. Left: ΔH = 399 gauss; T = 361°C. Right: ΔH = 330 gauss; T = 462°C.

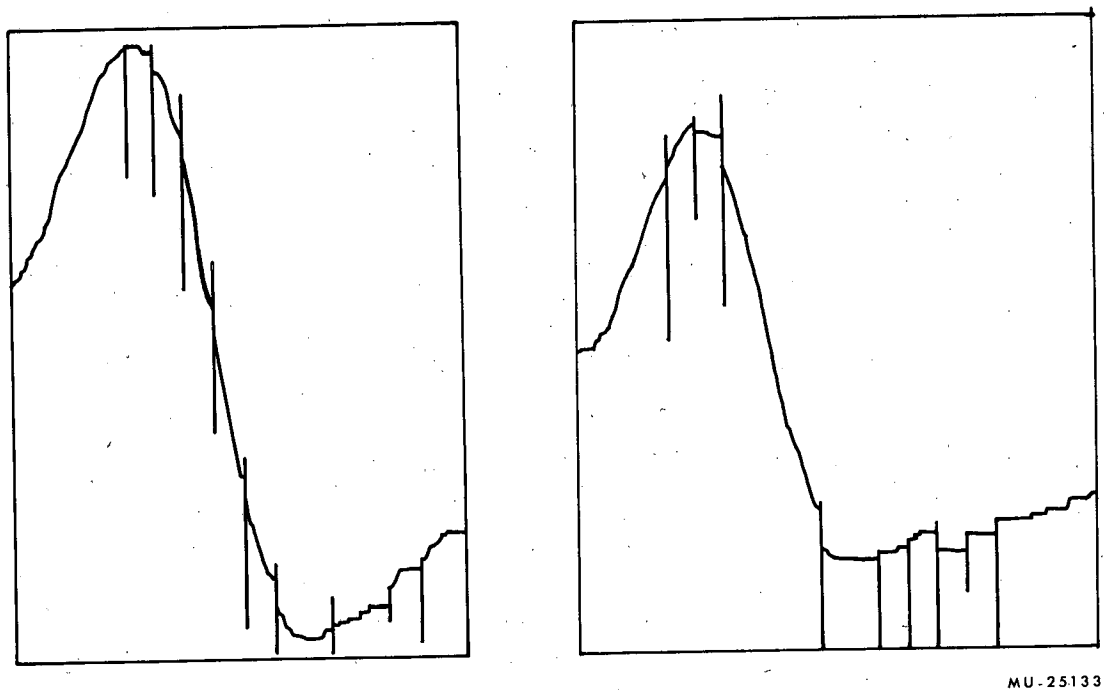

Fig. 28. $MnCl_2$ in $ZnCl_2$, 5.4 mole% (1 M). Smallest interval between frequency markers = 70.5 gauss. Left: ΔH = 421 gauss; T = 372°C. Right: ΔH = 370 gauss; T = 442°C.

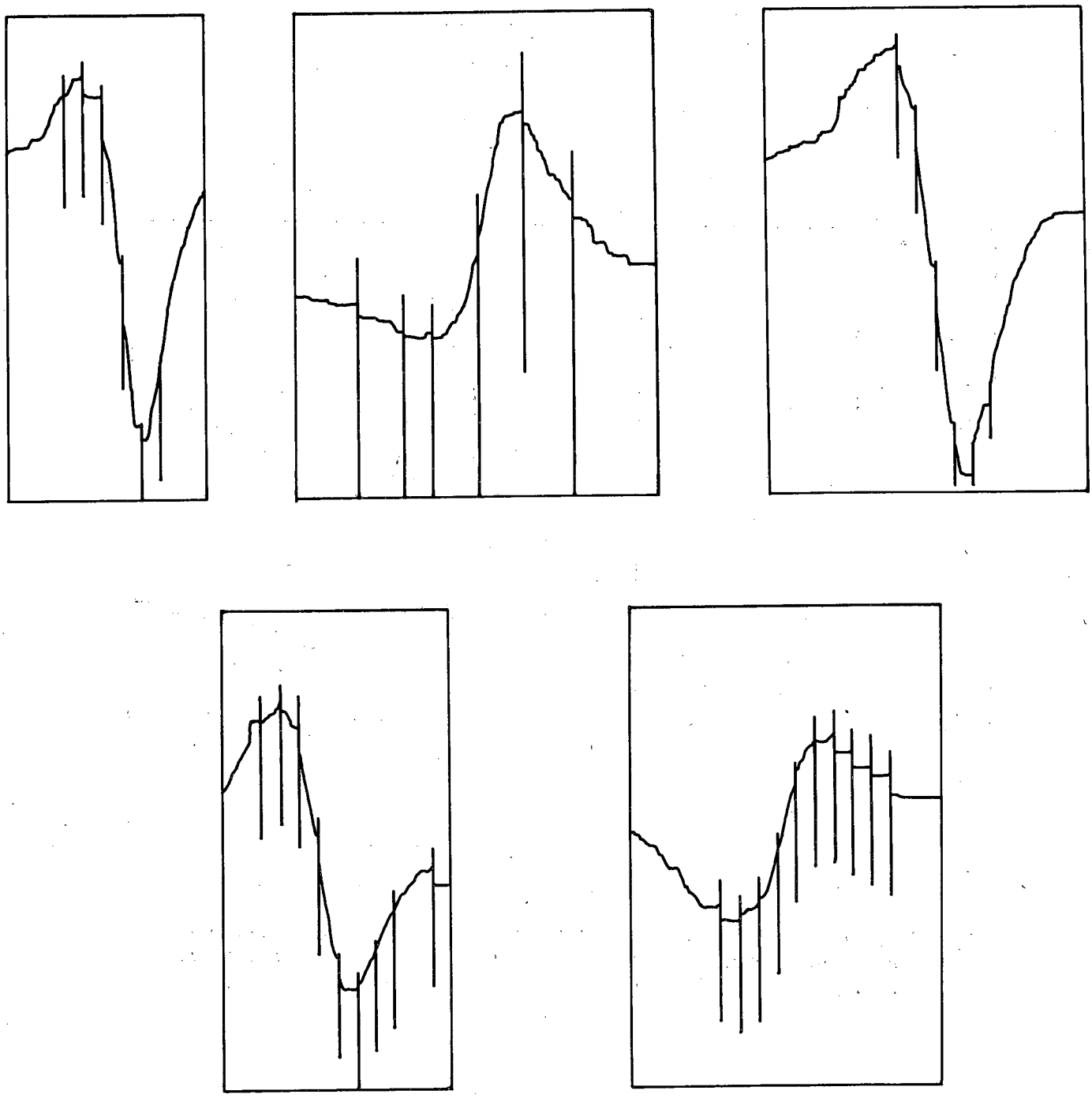

MUB-866

Fig. 29. Line shapes of Cr(III). Above: left, 1.5 mole% (0.5 M); $CrCl_3$ in LiCl-KCl; ΔH = 1.61 gauss; T = 355°C; 47.0 gauss between frequency markers. Center, 2.8 mole% (1 M) $CrCl_3$ in LiCl-KCl; ΔH = 129 gauss; T = 333°C; 70.5 gauss between frequency markers. Right, 5.4 mole% (1 M); $CrCl_3$ in $ZnCl_2$; ΔH = 97 gauss; T = 348°C; 23.5 gauss between frequency markers.
Below: left, ΔH = 81 gauss; T = 25°C. Right, ΔH = 112 gauss; T = 173°C. 23.5 gauss between frequency markers.

D. Discussion

1. Liquids

Resonances were observed only in solutions of Mn^{++} and Cr^{+3}. A possible explanation is that the ground state is an orbital singlet* for these ions. Thus there would be only a small broadening effect from the spin-orbit coupling and dipole-dipole interaction, which would be due to mixing of the ground-state wave function with far removed excited states. An exception to this hypothesis is Ni^{+2}, whose ground state in a cubic crystal field is also an orbital singlet. However, no resonance has been observed in water solutions of this ion, presumably because of the large axial term.[24]

The line width in solutions of $MnCl_2$ in $ZnCl_2$ is approximately the same above and below the melting point. This is consistent with the properties of $ZnCl_2$ reported by Mackenzie and Murphy.[32] The viscosity just above the melting point was found to be greater by a factor of 500 than that of most other metallic halide melts. Thus it was concluded that there is a much greater degree of association in liquid $ZnCl_2$, and it is structurally similar to the solid at the melting point.

The continuity of the line width vs temperature in passing through the melting point is more difficult to interpret for the solutions of $CrCl_3$ in LiCl-KCl eutectic. It is possible that colloidal suspensions rather than true solutions were formed. This would also explain the constancy of the line width in the liquids with decreasing viscosity (increasing temperature). We can only say that the liquid samples appeared to be homogeneous violet solutions. If, indeed, true solutions were formed, the relaxation mechanism in the liquids must be the same as that for the solids.

The temperature dependence of the line width or relaxation times is compared with theoretical predictions in Figs. 30 through 32 for the manganese systems. The line widths were taken from Figs. 12 and 14, and the relaxation time T_2 was calculated from $\Delta H = (2/\sqrt{3})\,(1/\gamma T_2)$. This assumes a Lorentzian line shape, which is approximately what was observed.

The Al'tshuler and Valiev theory predicts

$$\Delta H \propto \frac{1}{\sqrt{T}} \quad \text{for} \quad kT \ll \hbar\omega_v , \tag{1}$$

where ω_v is an average vibrational frequency. From Fig. 30 it is apparent that the agreement with this theory is rather poor, especially in the case of $MnCl_2$-LiCl-KCl. At higher temperatures the $MnCl_2$-$ZnCl_2$ data do seem to fall upon the theoretical straight line. However, this appears a bit strange to us, for it is in this region that the liquid $ZnCl_2$ is becoming more ionic, making a vibrational relaxation mechanism improbable.

*The seven-fold orbital degeneracy of Cr^{+++} is split by a cubic crystal field with an orbital singlet lying lowest.

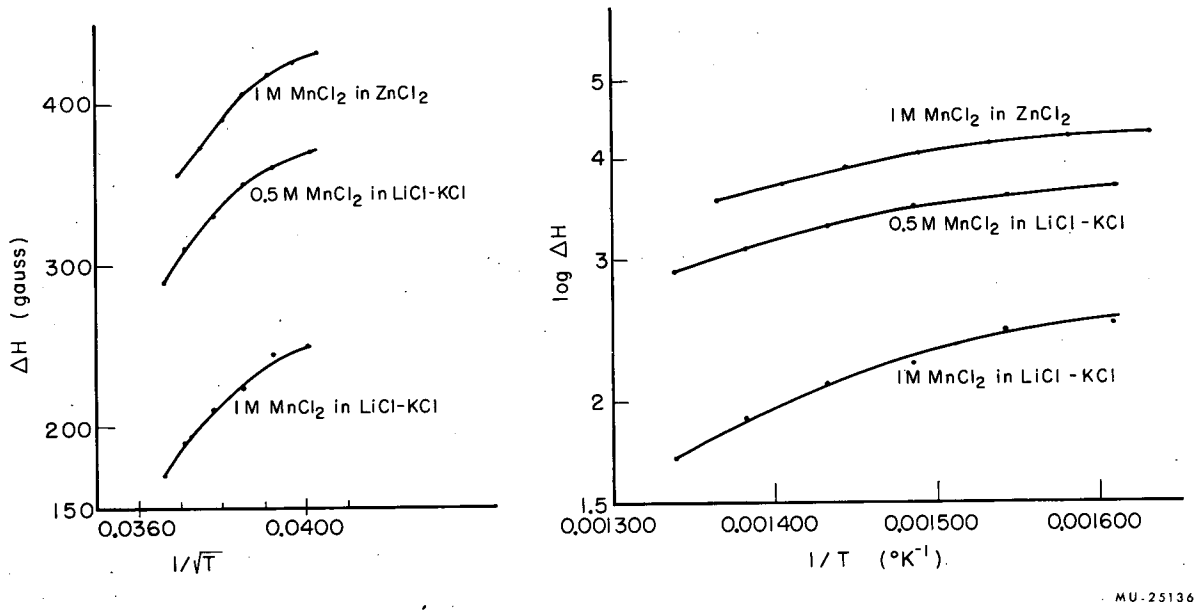

Fig. 30. Comparison to theories of Al'tshuler and Valiev (left) and Bloembergen and Morgan (right).

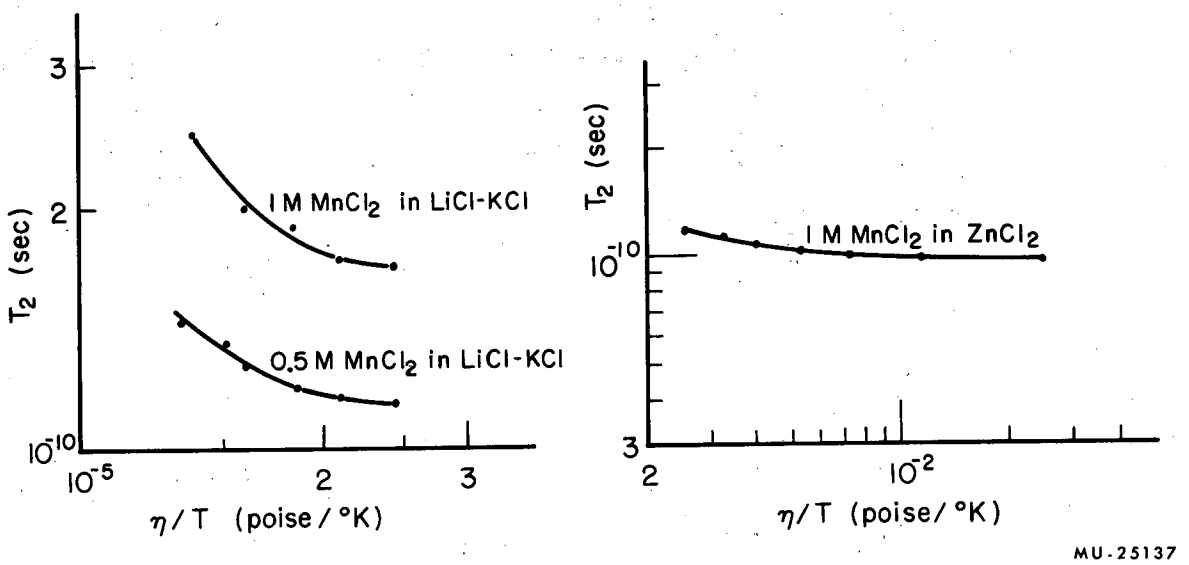

Fig. 31. Comparison to theory of Bloembergen, Purcell, and Pound.

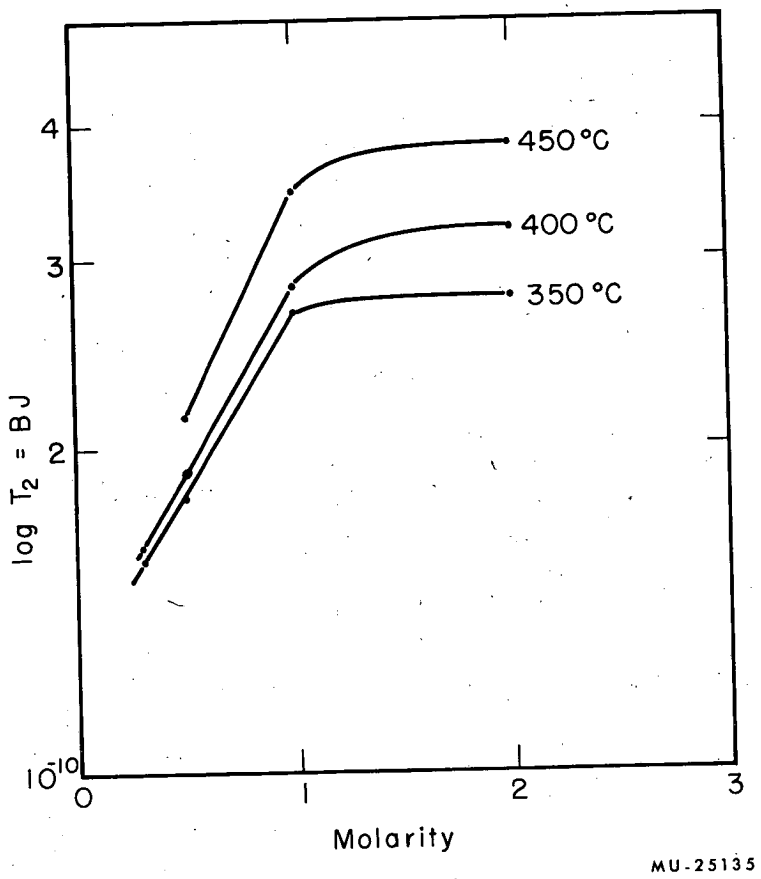

Fig. 32. Concentration dependence of the exchange integral.

Bloembergen and Morgan predict an electron spin relaxation time

$$\frac{1}{\tau_s} = \frac{12 C_2^2 h^{-2}}{5S(S+1)} \left[\frac{\tau_v}{1+\omega_s^2 \tau_v^2} + \frac{4\tau_v}{1+4\omega_s^2 \tau_v^2} \right]. \qquad (2)$$

Here τ_v is the correlation time for the impact of the solvent upon the solvated ion and W_s is the electron spin resonance frequency. For Mn^{++},

$$C_2^2 = \frac{2}{225} (2S+1) S^2 (S+1)^2 \left\{ 1 - \left[\frac{3}{4} S(S+1) \right] \right\} \left[2 \left\langle D^2 \right\rangle_{Av} + 3 \left\langle E^2 \right\rangle_{Av} \right],$$

which is temperature-independent if we assume that the crystal field parameters D and E do not vary appreciably with temperature.

If we further assume $\omega_s^2 \tau_v^2 << 1$,* then the line width should be directly proportional to τ_v. This quantity is expected to be of the form

$$\tau_v = \tau_v^0 \exp\left(\frac{V_v}{RT} \right). \qquad (3)$$

Thus, a plot of ln $1/T_2$ against $1/T$ should give a straight line of slope V_v/R. It can be seen in Fig. 30 that the agreement is not especially good. However, an estimate of V_v from the data for 1 M $MnCl_2$ in LiCl-KCl at 394°C and 442°C gives 3.3 kcal/mole, which is surprisingly close to Bloembergen and Morgan's value of 3.9 kcal/mole found for aqueous solutions.

According to the early work of BPP,[3] the general formula for spin-lattice relaxation is

$$\frac{1}{T_1} = \frac{3}{2} \gamma^4 \hbar^2 I(I+1) \left[J_1(\nu_0) + \frac{1}{2} J_2(2\nu_0) \right], \qquad (4)$$

where $J_1(\nu_0)$ and $J_2(2\nu_0)$ are spectral densities, and all other symbols have their usual meanings. Since J_1 and J_2 are Fourier transforms of correlation functions, it can be shown that

$$J_1(\nu_0) \propto \frac{\tau_c}{1+\omega_0^2 \tau_c^2} \quad \text{and} \quad J_2(2\nu_0) \propto \frac{2\tau_c}{1+4\omega_0^2 \tau_c^2}. \qquad (5)$$

Here τ_c is the correlation time and is a measure of the time over which the value of a function is related to its value at an earlier time. For the rotational averaging of a sphere of radius a in a viscous medium

$$\tau_c = 4\pi\eta a^3/3kT, \qquad (6)$$

*Bloembergen and Morgan predict $\tau_v = 2 \cdot 10^{-12}$ sec at room temperature.

where η is the viscosity. We find from Eq. (6) that for $ZnCl_2$ and LiCl-KCl* at 400°C, τ_c takes on the values $6.6 \cdot 10^{-10}$ sec and $2.3 \cdot 10^{-12}$ sec, respectively. Thus at microwave frequencies for the LiCl-KCl system, we have

$$\omega_0^2 \tau_c^2 \ll 1,$$

and it can be seen from Eq. (5) and Eq. (4) that a plot of log T_1 against log $\frac{\eta}{T}$ should yield a straight line of slope -1.

For the averaging of the local field due to translation of neighbors one finds

$$\frac{1}{T_1} \propto \frac{1}{D},$$

where D is the diffusion constant. Stokes' s relation gives

$$D = \frac{kT}{6\pi \eta a},$$

so this mechanism predicts a similar relationship between T_1 and $\frac{\eta}{T}$.

We have plotted log $T_2 (T_1 \approx T_2)$ vs log $\frac{\eta}{T}$ for the $MnCl_2$-LiCl-KCl system in Fig. 31, and find that the agreement is better at higher temperatures. At the lower temperatures $(\omega_0 \tau_c)^2$ is larger; however, it is only 0.032 at the lowest temperature included (350°C). Thus, it is doubtful that we are approaching the region in which T_1 increases with $\frac{\eta}{T_c}$. Cf. Ref. 3, Fig. 14.

For the $ZnCl_2$ system $\omega_0^2 \tau_c^2 \approx 1500$ at 400°C, so that the line width parameter T_2 approximately equals T_2'', the relaxation time due to spin-spin interactions unmodified by spin lattice interactions. From Fig. 31 it can be seen that T_2 is approximately constant at lower temperatures, in agreement with the behavior predicted by Fig. 14 of Ref. 3.

The comparison of our results with Kivelson' s Theory is slightly more difficult to make owing to the large number of parameters involved and complicated functional form of the expression for the line width. It is believed that for our case the most appropriate of his expressions is

$$\Delta H_{1/2} = -\left\{A^2 \tau^1 + A^2 \tau_n^1 + \frac{1}{6} \sigma_{IS}^2 \tau_c 55 (1 - \tau_c^2 \omega_e^2)\right\}\left(\frac{1}{3}\right) J(J+1)$$

$$+ \left\{\sigma_{SS}^2 \tau_c \frac{5}{2} (1 - \tau_c^2 \omega_e^2)\right\} S(S+1). \qquad (7)$$

*The viscosity of the eutectic mixture is estimated from data in C. J. Smithells, Metals Reference Book, Vol II (Interscience Publishers, Inc., New York, 1955). These data on other alkali halides at equal increments above their melting points had only a small variation among themselves.

The quantities appearing in this expression are defined as follows:

A = hyperfine coupling constant $\approx$ 95 gauss for Mn^{++} in aqueous solution,

$\tau^{-1} = \dfrac{(3\pi)^{1/2}}{2J[S(S+1)]^{1/2}}$, where J is the exchange integral,

$\tau_n^{-1} = \dfrac{(3\pi)^{1/2}}{2[S(S+1)]^{1/2}J} \exp[-3\gamma^2\hbar^2/4S(S+1)J^2]$,

σ_{IS}^2 = second moment arising from the nuclear-electronic dipolar interaction,

τ_c = the correlation time,

$\omega_e^2 = \frac{2}{3}S(S+1)J^2$,

σ_{SS}^2 = second moment arising from the electronic-electronic dipolar interaction.

The effects of the exchange interaction, the hyperfine interaction, the nuclear-electronic and electronic-electronic dipolar interactions, and the motional Hamiltonian are included. We find upon expressing Eq. (7) as a function of J that only the first term is significant,* which would be expected with strong motional narrowing. Thus the line width is predicted to be inversely proportional to the exchange integral.

This behavior is equivalent to that derived by other workers for the narrowing of a resonance line by molulation of the perturbing term which determines the line width. That is, Anderson found

$$\Delta\omega = \omega_p^2/\omega_e , \tag{8}$$

where $\Delta\omega$ is the half width at half power, ω_p^2 the second moment of the line, and ω_e is proportional to J.[25] BPP predicted the same behavior with ω_p representing the frequency amplitudes of the perturbations and ω_e the rate of motion.

Although we cannot test meaningfully the validity of Kivelson's calculation, we shall use his and, a fortiori, Anderson and Weiss' s prediction of the inverse proportionality of line width and exchange integral to estimate the concentration dependence of the exchange integral. Equation (8) is equivalent to

$$T_2 = BJ, \tag{9}$$

*The first two terms are identical to Kivelson's Eq. (73) in his 1960 paper for the case of high concentration and strong exchange and motional effects.

where B is a proportionality constant. At a given temperature the exchange integral should be a function of concentration alone. We find (see Fig. 32) that a plot of log T_2 vs concentration for the $MnCl_2$-LiCl-KCl system gives a straight line over the concentration range 0.3 M to 1 M. We can thus predict

$$J = De^{0.796C},$$

where C is the molar concentration and D is a constant which is a function of B. Apparently, the exchange integral has ceased to vary rapidly with concentration in the range 1 M to 2 M, indicating that the maximum exchange contribution is being made. In addition, it should be mentioned that a linear dependence of J on concentration also gives a fairly good fit to the experimental data over this concentration range; however, it is not so good as the exponential dependence.

The exchange integral between a pair of nearest neighbors can be written

$$J_{12} = -2S\int \frac{a(1)b(1)}{R_{a1}}\, d\tau_1 + \frac{S^2}{R_{ab}} + \iint \frac{a(1)b(2)b(1)a(2)}{r_{12}}\, d\tau_1 d\tau_2 ,$$

where S is the overlap integral and a(1) and b(1) are nonorthogonal electron orbitals centered on nuclei a and b respectively. From this it can be seen that J is a sensitive function of the interelectronic and interionic distances involved and of the overlap of the wave functions.

What we should like to know is the concentration dependence of J. But the only term that can be easily estimated is R_{ab}. This distance between neighboring nuclei would be proportional to $(\text{concentration})^{-1/3}$ if the ions occupied sites on a simple cubic lattice. However, even if the entire calculation were performed, assuming some interionic distances fixed at a given concentration, it would not be of any significance owing to the Browian motion in a liquid. We are therefore unable to make any sort of theoretical estimate of J (concentration) to compare with our experimental results.

The comparison of the $MnCl_2$-LiCl-KCl and $MnCl_2$-H_2O systems (see Fig. 11)is quite interesting in view of the great difference in line widths at various concentrations. At low concentrations the relaxation in water solutions is determined by the spin-orbit coupling according to Ref. 30; in any case the interactions are weak, since the line is narrow. In contrast, the line width in the molten salts is increasing rapidly with dilution at a concentration of 0.3 M. It is difficult to ascribe a definite relaxation mechanism; however, the interaction with oscillating magnetic fields due to the ionic environment (Cf. Chap. I Part A) seems most plausible to us. We might also postulate a relaxation mechanism via the impinging solvent ions. These could form short-lived complexes with the paramagnetic ions, with a decrease in relaxation time due to uncertainty-principle broadening. From $\Delta E\, \Delta t \gtrsim \hbar$ it can be easily shown that a lifetime of approx 10^{-11} sec would give rise to a line width of 1000 gauss.

In the concentrated molten salt solutions there is obviously a strong exchange interaction which narrows the line considerably. The line width in the concentrated water solutions is probably due to spin-spin interactions with neighboring Mn^{++} ions. The weaker exchange interaction in the water solutions might be explained by differences in complex formation. The manganese is probably in the form of $Mn(H_2O)_6^{++}$ in water solutions, whereas it is likely that Mn(II) is only weakly coordinated, if at all, with Cl^- ions in the molten salts. The coordination sphere of water molecules might thus prevent the exchange integral from taking on an appreciable value.

We do not believe that any of the present theories of relaxation in liquids give an adequate explanation for our results. Our use of the proportionality of T_2 and J was not intended to imply any confidence in Kivelson's treatment. Since deviations from g = 2.00 were observed, an applicable theory of relaxation would almost certainly have to include the spin-orbit coupling interaction. The only mechanism which we can definitely identify from our studies is that of exchange narrowing at high concentrations. The temperature dependence at a given concentration might be described by the simple BPP theory. However, this decreasing line width as a function of temperature might also be explained by a more effective exchange interaction with lower viscosity.[33]

It is our belief that the BPP treatment of relaxation in liquids, even with its restriction to a consideration of the dipolar interaction alone, is still as good as (or better than) any of the more sophisticated papers published in the literature in the past decade.

We believe that the principal value of this work is in indicating a method of attack and the order of magnitude of the results to be expected in future more detailed studies of molten salt solutions.

2. Solids

Data on the crystal structures of these various compounds and the results of previous ESR measurements on the undiluted powders are found in Tables V and VI. These data are compared with our results in the following discussion. Also, cf. Table III in Part C.

a. $MnCl_2$ in LiCl-KCl

ESR studies of single crystals of NaCl, KCl, and LiCl doped with Mn^{++} have been reported by several workers. It has been found that Mn^{++} exists in different environments which depend upon the sample treatment prior to measurement and on the concentration of Mn^{++}. We mention here only the most pertinent of these results.

The original work was performed by Forrester and Schneider,[34] who found a single line of width 26 to 35 gauss for Mn^{++} in KCl crystals grown from the melt. If the crystals were grown from aqueous solution six hyperfine lines were observed each having a width of 29 gauss. Upon annealing at 500°C these lines disappeared irreversibly to give the single line characteristic of crystals grown from the melt. This line was identified with $MnCl_2$ aggregates near an internal boundary and it was believed that

Table V. Crystal structures

Compound	Structural type	Symmetry of metal ion wrt anions	Reference
$MnCl_2$	Hexagonal (Rhombohedral)	Octahedral	R. W. G. Wyckoff, Crystal Structure I (Interscience Publishers, Inc., New York, 1948).
$ZnCl_2$	Hexagonal (Rhombohedral)	Octahedral	"
$FeCl_3$	Hexagonal (Rhombohedral)	Octahedral	"
$CrCl_3$	Hexagonal (Rhombohedral)	Octahedral	"
$NiCl_2$	Hexagonal (Rhombohedral)	Octahedral	"
$MnCl_2 \cdot 4H_2O$	Monoclinic	-	Ibid, Volume III
LiCl	Face-centered cubic	Octahedral	
KCl	Face-centered cubic	Octahedral	

Table VI. Summary of previous ESR measurements

Compound	ΔH (gauss)	g	Frequency (Mc)	Reference
$CrCl_3$	79	1.997	10,000	Y. Ting, L. D. Farringer, and D. Williams, Phys. Rev. 97, 1037 (1955).
$NiCl_2$	682	2.25	10,000	J. W. Leech and A. J. Manuel, Proc. Phys. Soc. (London) B69, 210 (1956).
$MnCl_2 \cdot 4H_2O$	400	2.00	24,120	F. W. Lancaster and W. Gordy, J. Chem. Phys. 19, 1181 (1952).
$VOCl_2$	72	2.00	24,138	F. W. Lancaster and W. Gordy, J. Chem. Phys. 19, 1181 (1952).
$MnCl_2$	723	-	-	H. Kumagai, K. Ono, and J. Hayashi, Phys. Rev. 85, 925 (1952).

the hyperfine structure was suppressed by exchange effects. The orientation-independent hyperfine lines were believed to arise from the $m_s = 1/2 \leftrightarrow -1/2$ transitions of isolated Mn^{++} ions in the cubic lattice.

Fukuda found three types of behavior in KCl/Mn grown from the melt:[35]
(a) overlapping lines with $\Delta H = 30$ gauss and 100 gauss after annealing,
(b) a single line with $\Delta H = 30$ gauss after quenching from 300°C to 500°C, *
(c) six hyperfine lines each of $\Delta H = 30$ gauss after quenching from 500°C.

A very thorough and direct study of temperature effects in doped crystals of LiCl, KCl, and NaCl grown from the melt was made by Watkins.[36] He observed the transformations of the spectra upon heating the sample in situ to a temperature of 600°C. The species were identified as follows:

I. $\Delta H = 130$ gauss -- This arises from exchange-narrowed clusters.

II. Six orientation-independent hyperfine lines -- These are due to isolated Mn^{++} ions.

III_1 and III_2. Complex orientation-dependent spectra -- Species III_1 was identified as a Mn^{++} ion associated with a positive ion vacancy in the nearest cation site, while III_2 is supposedly an association of Mn^{++} with a vacancy in the next nearest cation site. These species were identified by symmetry considerations.

IV. Complex orientation-dependent spectrum of low intensity -- This was said to arise from Mn^{++} associated with a doubly charged negative impurity in one of the nearest Cl^- sites.

Only species III_1 and III_2 were studied in LiCl and KCl. In KCl Watkins observed, in addition, a 26-gauss line which was identified as Mn^{++} in K_4MnCl_6 crystals. The basis of this identification was that this narrow line was observed with high intensity only in cloudy portions of the crystals. We should like to see this hypothesis substantiated by an x-ray analysis.

We shall now attempt to interpret our results in view of the previous analyses. The species that contribute to the hyperfine structure appearing at approximately 180°C certainly include II described above. We have averaged Watkins' s spin Hamiltonian over angles as is appropriate for a powder and find that III_1 and III_2 would also contribute to the six-line hyperfine pattern. Thus the temperature effects are easily understood.

The concentration-independent 27-gauss line in the unmelted powders and 170-gauss line in the samples melted prior to measurement at room temperature are more difficult to identify. One would expect the mixed powder (unmelted) to give rise to a spectrum identical to that of $MnCl_2$. However, it was found to differ in line width by more than an order of magnitude. The 27-gauss line width is almost identical to that identified by Watkins as arising from K_4MnCl_6. But we believe it improbable that the drying procedure could yield mixed crystals. Also, this narrow line was observed in a sample of $MnCl_2$ in LiCl alone. We could find no reference to mixed crystals formed from these latter two compounds, and conclude that they do not exist. This makes the mixed-crystal hypothesis even more improbable as an explanation for our results.

*This has also been observed by H. Yoshimura, J. Phys. Soc. Japan 15, 435 (1960).

We believe that this 27-gauss-wide line with no observable hyperfine structure must arise from exchange-narrowed clusters. However, the disparity with the pure $MnCl_2$ results would have to be explained by postulating a different structural arrangement such that the Mn^{++}-Mn^{++} distance is smaller. This would increase the exchange integral and thus decrease the line width. We have verified that it is the drying procedure which is responsible for the narrow line (cf. Table III). Therefore it is probably via a diffusion mechanism that the above arrangement occurs. We might even postulate that the $MnCl_2$ diffuses onto the surface of the LiCl and KCl crystals to occupy positions such that the interionic distances between manganese ions are small.

Since the 170-gauss line in the melted samples at room temperature was concentration-independent (except for the 0.3 mole % sample), it must also arise from exchange-narrowed manganese clusters which are not uniformly distributed in the host lattice. Apparently, the melting procedure results in some mixing of $MnCl_2$ with the host lattice which increases the Mn^{++}-Mn^{++} distance relative to that in the dried powders. The faintly perceptible hyperfine structure in Figs. 22 and 23 implies that a small amount of Mn^{++} exists as species II, III_1, and (or) III_2.

b. $MnCl_2$ in $ZnCl_2$

It is likely that the disparity of the unmelted samples from those above simply reflects a difference in the properties of $ZnCl_2$. This compound is very deliquescent. Therefore, the grinding procedure probably resulted in the absorbtion of waters of hydration by $MnCl_2$. This water would have been driven off during the drying procedure, leaving the Mn^{++} in a rather unsymmetrical environment as evidenced by the excess line width. The narrower line in the melted samples probably indicates that the Mn^{++} was incorporated in octahedral sites in the $ZnCl_2$ lattice.

c. $MnCl_2$ and $MnCl_2 \cdot 4H_2O$

Our room-temperature value of $\Delta H = 860$ gauss for $MnCl_2$ exceeds that of Kumagai's previous measurement. See Table VI. The decrease in line width with increasing temperature is probably due to motional narrowing by modulation of crystal-field parameters.

For $MnCl_2 \cdot 4H_2O$ at room temperature we found $\Delta H = 480$ gauss, in contrast to Gordy's value of 400 gauss at 24120 Mc. The small variation in line width with temperature found for this hydrated compound is probably due to its being shielded from the crystal field by its waters of hydration. This shielding might also account for the small value of the room-temperature line width of $MnCl_2 \cdot 4H_2O$ relative to $MnCl_2$. In this case the shielding would decrease the effectiveness of the spin-spin interactions as a broadening mechanism.

d. $CrCl_3$ and $CrCl_3$ in LiCl-KCl and in $ZnCl_2$

The mixed compounds show the expected behavior if it is assumed that the $CrCl_3$ is homogeneously incorporated into the host lattice. The decreasing line width as a function of increasing concentration is, of course, due to exchange narrowing:

Our room-temperature value of $\Delta H = 77$ gauss for $CrCl_3$ compares quite well with Williams' s previous measurement. However, his g value of 1.997 exceeds our room-temperature measurement of 1.975 ± 0.005. The increase in line width beginning at approximately 240°C could be due to spin-phonon interactions. A linear dependence of line width on temperature is predicted for the direct processes.[37]

e. $NiCl_2$ in LiCl-KCl and $FeCl_3$ in LiCl-KCl

These are the only remaining compounds in which the relaxation properties appeared strongly temperature-dependent. The line widths at room temperature are probably due to spin-spin interactions as modified by the exchange interaction.

Powdered $NiCl_2$ was previously studied by Leech and Manuel,[38] who found variations in the line width and g value as a function of temperature from 20°K to room temperature. We might therefore have expected to find variations in these quantities in our experiments on $NiCl_2$ in the LiCl-KCl lattice at temperatures of 25°C and above.

For 3.0 mole % $NiCl_2$ in LiCl-KCl, the rapid decrease in line width as a function of increasing temperature might again be due to motional narrowing, as for $MnCl_2$. The reduction in the g shift over this temperature range offers a mechanism for this decrease in line width. The g shift is determined by the spin-orbit interaction, which must here be decreasing. Thus the spin-phonon interaction would become less effective as a relaxation mechanism and could lead to a decrease in line width such as we observed.

Actually Ni^{++} is in the same valence state as Mn^{++} and has a radius of 0.70 A compared to 0.80 A for Mn^{++}. We might therefore have a complicated situation involving Ni^{++} ions in different environments similar to that which was observed for Mn^{++}.

The very marked increase in line width at 240°C for the $FeCl_3$-LiCl-KCl system is puzzling to us, especially in view of the small variation exhibited by the undiluted $FeCl_3$. We are tempted to say that the sample was premelting even though it appeared to be solid at this temperature. Apart from this highly speculative hypothesis, we can offer no explanation.

The above discussion of the temperature effects in solids is admittedly incomplete. As was mentioned earlier, these effects were somewhat incidental to the main purpose of this work. We should therefore prefer that this section on solids be considered primarily as a report of our experimental results.

ACKNOWLEDGMENTS

I am very grateful

To Professor Kenneth S. Pitzer, whose amazing physical insight, breadth of knowledge, and continual diligence and scientific enthusiasm have provided a constant source of inspiration, for his patience, aid and encouragement;

To Professor Rollie J. Myers, for many hours of profitable discussion, for many very helpful suggestions which were largely responsible for the success of this research, and especially for his continued interest in the problem which alleviated numerous periods of discouragement;

To Mr. Loren Cadre for his excellent technical assistance, his helpful advice, and his friendship;

To Dr. Juana Acrivos for many discussions and many pertinent references;

To Woodrow Wilson Foundation, The National Science Foundation, and The Atomic Energy Commission for their generous financial support.

APPENDIX

DISCUSSION OF THE ESR LINE SHAPE IN CONDUCTING MEDIA

To facilitate an understanding of the results of Chapters I and III, some discussion of the magnetic resonance phenomenon in conductors is necessary. Ordinarily, ESR measurements are made upon samples of dimensions less than the skin depth, and the power absorbed per unit volume is

$$P = 2H_1^2 \omega \chi'' ,$$

where H_1 is the rf field, ω the frequency, and χ'' the imaginary part of the susceptibility. That is, the power absorbed is directly proportional to χ'', and the experimentally observed quantity is

$$\frac{dP}{dH} \quad \text{or} \quad \frac{d\chi''}{dH} ,$$

where H is the dc magnetic field.

The problem of conducting media was first considered by Bloembergen.[39] The losses for an infinite plane sheet of thickness d (where $d \lesssim \delta$) in the presence of a tangential rf magnetic field were found by a solution of Maxwell's equations subject to the appropriate boundary conditions. It was thus shown that, for the case $d \gg \delta$, where δ is the skin depth, the magnetic resonance absorption is proportional to $(\chi'' + \chi')$. Here χ' and χ'' are the real and imaginary parts of the frequency-dependent susceptibility. This leads to an asymmetric absorption line and is applicable for the case of slowly diffusing dipoles.

A very elaborate theory taking spin diffusion into account has since been worked out by Dyson[40] for the case of a flat metal plate of arbitrary thickness. A relationship between $\vec{M}$ and $\vec{H}_1$ where both are functions of $\vec{H}$ was obtained; then a self-consistent set of solutions of Maxwell's equations with this relationship was found. Here $\vec{M}$ is the macroscopic magnetization, $\vec{H}_1$ the rf magnetic field, and $\vec{H}$ the static field. From the power absorbed by the metal, the line-shape function was obtained for different values of the parameters in Dyson's theory: T_D = time required for an electron to diffuse through the skin depth, T_1 = electron spin relaxation time, and T_T = time required for an electron to traverse the sample.*

Feher and Kip[13] brought Dyson's equations to a more usable form and made extensive comparisons with their own experimental results, which were in quite good agreement. It was also shown (see Fig. 33) how the theory can be utilized to obtain accurate g values and relaxation times from an observed resonance curve.

---

*This notation follows that of Ref. 13.

We found this figure somewhat ambiguous in our initial attempts to extract information from it. Accordingly, a more detailed analysis was performed for the case

$$\frac{T_D}{T_2} >> 1, \quad T_T >> T_D, \text{ and } T_T >> T_2.$$

This is the $d > \delta$ case with slowly diffusing dipoles.*

Here

$$p = \left[\frac{\omega H_1^2}{4} (\delta A)\, \omega_0 \chi_0 T_2\right] \left(\frac{1}{2}\right) \frac{1 - T_2(\omega - \omega_0)}{1 + T_2^2(\omega - \omega_0)^2}$$

and

$$\frac{dP}{d\omega} = \left[\frac{\omega H_1^2}{4} (\delta A)\, \omega_0 \chi_0 T_2\right] \left(\frac{T_2}{2}\right) \frac{T_2^2(\omega - \omega_0)^2 - 2T_2(\omega - \omega_0) - 1}{[1 + T_2^2(\omega - \omega_0)^2]^2} ;$$

P is the power absorbed by the sample and A the sample area; all other symbols have their usual definitions.

The results are found in Fig. 33 together with Feher's Fig. 5. The difficulty in utilization of his graph lies in the fact that it is drawn for the particular case in which the resonance point coincides with the half-power point. On our graph it seems clearer to what quantities the definitions of ΔH and δH actually refer. Included in Fig. 33 is a plot of A/B vs $(T_D/T_2)^{1/2}$,† which in turn yields $\gamma \Delta H T_2$ and $\gamma \delta H T_2$. These values and the experimentally determined quantity ΔH then give δH, which makes it quite simple to obtain T_2 and the g value.

For reference in Chapter III a comparison of the line width ΔH_{pp}§ between points of maximum slope on the derivative curve for samples greater

*See Ref. 13, Eqs. (3.7) and (3.8). Equation (3.7) is identical to Bloembergen's Eq. (8) using the definition of the Bloch susceptibilities except for a constant term (Ref. 39); this term was not investigated, as the experimentally observed quantity is the derivative of power absorbed.

†According to Feher these values are not in exact agreement with the result of a calculation of T_D from resistivity data; but in the absence of the latter, e.g., for the case of a molten salt dissolved in a metal, the above procedure must be followed.

§We use the notation ΔH_{pp} (peak to peak) to avoid confusion with the ΔH above, the line width at half-power points. This notation is followed only in this appendix.

than and less than the skin depth is included. For slowly diffusing dipoles, the situation encountered in a molten salt, the graph in Fig. 33 is applicable, and we see

$$\Delta H_{pp} = 1.27/\gamma T_2 \qquad (\text{for } d > \delta),$$

whereas for a Lorentz line,

$$\Delta H_{pp} = (2/\sqrt{3})\,(1/\gamma T_2) = 1.16/\gamma T_2 \quad (d < \delta),$$

a difference of less than 10%.

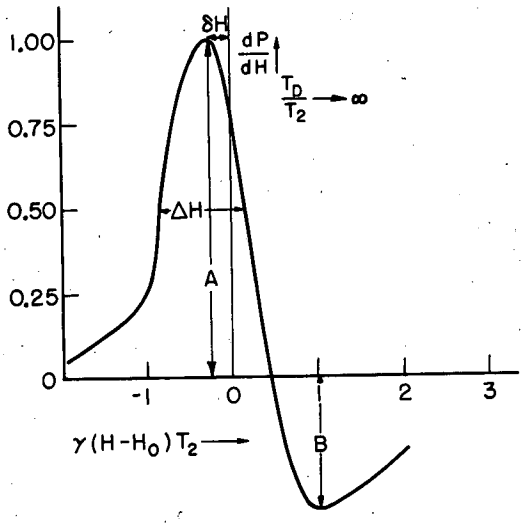

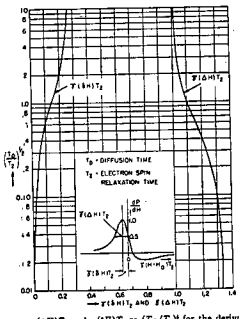

$\gamma(\Delta H)T_2$ and $\gamma(\delta H)T_2$ vs $(T_D/T_2)^{\frac{1}{2}}$ for the derivative of the power absorption due to electron spin resonance in thick metal plates.

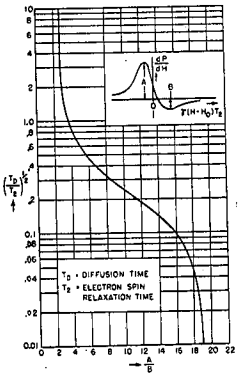

A/B vs $(T_D/T_2)^{\frac{1}{2}}$ for the derivative of the power absorption due to electron spin resonance in thick metal plates.

MU-25114

Fig. 33. Power absorbed at resonance by thick metal plates in the limit of slowly diffusing dipoles (left). Figures at right reproduced from Ref. 13.

REFERENCES

1. G. E. Blomgren and E. R. Van Artsdalen, Ann. Rev. Phys. Chem. 11, 273 (1960);
   G. J. Janz, High Temperature Chemistry - A Tool for the Future (Stanford Research Institute, Menlo Park, California, 1956), p. 169;
   M. Bloom and J. O'M. Bockris, Modern Aspects of Electrochemistry No. 2 (Academic Press, New York, 1959).

2. J. D. Corbett, J. Am. Chem. Soc. 79, 3020 (1957).

3. N. Bloembergen, E. M. Purcell, and R. V. Pound, Phys. Rev. 73, 679 (1948).

4. S. Karpachev, A. Stromberg, and E. Jordan, Compt. rend. acad. sci. URSS 36, 101 (1942).

5. M. A. Bredig and J. W. Johnson, J. Phys. Chem. 64, 1899 (1960).

6. H. R. Bronstein and M. A. Bredig, J. Am. Chem. Soc. 80, 2077 (1958).

7. H. R. Bronstein, A. S. Dworkin, and M. A. Bredig, J. Chem. Phys. 34, 1843 (1961).

8. W. L. Jolly, Progr. in Inorg. Chem. 1, 235 (1959).

9. D. E. G. Austin, D. J. E. Ingram, and J. G. Tapley, Trans. Faraday Soc. 54, 400 (1958).

10. Carol G. Montgomery, Technique of Microwave Measurements (McGraw-Hill Book Company, Inc., New York, 1947), p. 297.

11. C. H. Townes and A. L. Shawlow, Microwave Spectroscopy (McGraw-Hill Book Company, Inc., New York, 1955), Chap. XIV.

12. L. S. Singer, Rev. Sci. Instr. 32, 213 (1961).

13. G. Feher and A. F. Kip, Phys. Rev. 98, 337 (1955).

14. H. R. Bronstein, A. S. Dworkin, and M. A. Bredig, in Chemistry Annual Progress Report, Oak Ridge National Laboratory Report ORNL-2983, June 20, 1960, p. 64.

15. W. T. Doyle, D. J. E. Ingram, and M. J. A. Smith, Phys. Rev. Letters 2, 497 (1959).

16. W. Burton Lewis and F. E. Pretzel, J. Phys. Chem. Solids 19, 139 (1961).

17. R. A. Levy, Phys. Rev. 102, 31 (1956).

18. R. J. Elliott, Phys. Rev. 96, 266 (1954).

19. F. E. Pretzel and C. C. Rushing, J. Phys. Chem. Solids 17, 232 (1961).

20. F. Seitz, Revs. Modern Phys. 26, 7 (1954).

21. See Ref. 1; also Ann. N. Y. Acad. Sci. 79, Art. 11 (1960).

22. R. G. Hayes, Electron Spin Resonance Line Widths of Transition-Metal Ions and Complexes in Solution (Thesis), Lawrence Radiation Laboratory Report, UCRL-9873, September 1961 (unpublished).

23. H. M. McConnell, J. Chem. Phys. 25, 709 (1956).

24. B. R. McGarvey, J. Phys. Chem. 61, 1232 (1957).

25. For a discussion of the exchange phenomenon in solids, see P. W. Anderson and P. R. Weiss, Revs. Modern Phys. 25, 269 (1953); P. W. Anderson, J. Phys. Soc. Japan 9, 316 (1954).

26. D. Kivelson, J. Chem. Phys. 27, 1087 (1957); D. Kivelson, J. Chem. Phys. 33, 1094 (1960).

27. R. Kubo and K. Tomita, J. Phys. Soc. Japan 9, 888 (1954).

28. S. A. Al'tshuler and K. A. Valiev, Soviet Phys. JETP 35, 661 (1959).

29. J. H. Van Vleck, J. Chem. Phys. 7, 72 (1939).

30. N. Bloembergen and L. V. Morgan, J. Chem. Phys. 34, 842 (1961).

31. E. R. Van Artsdalen and I. S. Yaffe, J. Phys. Chem. 59, 118 (1955).

32. J. D. MacKenzie and W. K. Murphy, J. Chem. Phys. 33, 366 (1960).

33. G. E. Pake and T. R. Tuttle, Phys. Rev. Letters 3, 423 (1959).

34. P. A. Forrester and E. E. Schneider, Proc. Phys. Soc. (London) B69, 833 (1956).

35. K. Fukuda, Y. Uchida, and H. Yoshimura, J. Phys. Soc. Japan 13, 971 (1958).

36. G. D. Watkins, Phys. Rev. 113, 79 (1959).

37. See, for example, R. D. Mattuck and M. W. P. Strandberg, Phys. Rev. 119, 1204 (1960).

38. J. W. Leech and A. J. Manuel, Proc. Phys. Soc. (London) B69, 210 (1956).

39. N. Bloembergen, J. Appl. Phys. 23, 1383 (1952).

40. Freeman J. Dyson, Phys. Rev. 98, 349 (1955).

Information Division
sa